LA-UR- 99-992

Approved for public release; distribution is unlimited.

Title: REMOVAL OF VOLATILE ORGANIC COMPOUNDS (VOCs) BY ATMOSPHERIC-PRESSURE DIELECTRIC-BARRIER AND PULSED-CORONA ELECTRICAL DISCHARGES

Author(s): Louis A. Rosocha, P-24
Richard A. Korzekwa, LANSCE-9

Submitted to: Chapter for Nova Science Publishers Book "Electrical Discharges for Environmental Purposes: Scientific Background and Applications", E.M. van Veldhuizen, Editor

Los Alamos
NATIONAL LABORATORY

REPORT DOCUMENTATION PAGE

Form Approved
OMB No. 074-0188

1. AGENCY USE ONLY (Leave blank)	2. REPORT DATE	3. REPORT TYPE AND DATES COVERED
	1999	Book Chapter

4. TITLE AND SUBTITLE
Removal of Volatile Organic Compounds (VOCs) by Atmospheric-Pressure Dielectric-Barrier and Pulsed-Corona Electrical Discharges

5. FUNDING NUMBERS
N/A

6. AUTHOR(S)
Louis A. Rosocha and Richard A. Korzekwa

7. PERFORMING ORGANIZATION NAME(S) AND ADDRESS(ES)
Los Alamos National Laboratory

8. PERFORMING ORGANIZATION REPORT NUMBER
N/A

9. SPONSORING / MONITORING AGENCY NAME(S) AND ADDRESS(ES)
SERDP
901 North Stuart St. Suite 303
Arlington, VA 22203

10. SPONSORING / MONITORING AGENCY REPORT NUMBER
N/A

11. SUPPLEMENTARY NOTES

Chapter for Nova Science Publishers Book "Electrical Discharges for Environmental Purposes: Scientific Background and Applications."

12a. DISTRIBUTION / AVAILABILITY STATEMENT
Approved for public release: distribution is unlimited.

12b. DISTRIBUTION CODE
A

13. ABSTRACT ***(Maximum 200 Words)***

During the past decade, interest in gas-phase pollution control has greatly increased, arising from a greater respect for the environment, more attention to the impact of environmental pollution, and a larger body of regulations. A promising set of methods now being applied to gas-phase pollution abatement is non-thermal plasma (NTP) technologies. These plasmas are useful for generating highly reactive species (e.g., free radicals) which readily decompose entrained pollutants in atmospheric-pressure gas streams. Such plasmas can generate both oxidative and reductive radicals –showing promise for treating a wide variety of pollutants, in some cases simultaneously decomposing multiple species. In this chapter, we will discuss the removal of gas-phase volatile organic compounds (VOCs) by two types of electric-discharge-driven NTPs: dielectric-barrier (silent) discharges and pulsed corona discharges. These two types of discharges are easily operated at atmospheric pressure or above, thereby having a high process throughput compared to low-pressure NTPs.

14. SUBJECT TERMS
SERDP, SERDP Collection, VOCs, atmospheric-pressure dielectric-barrier, NTP, pulsed-corona electrical discharge

15. NUMBER OF PAGES
46

16. PRICE CODE
N/A

17. SECURITY CLASSIFICATION OF REPORT	18. SECURITY CLASSIFICATION OF THIS PAGE	19. SECURITY CLASSIFICATION OF ABSTRACT	20. LIMITATION OF ABSTRACT
unclass	unclass	unclass	UL

Nova Science Publishers Book
Electrical Discharges for Environmental Purposes:
Scientific Background and Applications

E.M. van Veldhuizen, Editor

Part 2: Applications
Chapter 10
Removal of Volatile Organic Compounds (VOCs) by Atmospheric-Pressure Dielectric-Barrier and Pulsed-Corona Electrical Discharges

Louis A. Rosocha and Richard A. Korzekwa
Los Alamos National Laboratory
Los Alamos, New Mexico (USA)

Abstract

During the past decade, interest in gas-phase pollution control has greatly increased, arising from a greater respect for the environment, more attention to the impact of environmental pollution, and a larger body of regulations. A promising set of methods now being applied to gas-phase pollution abatement is non-thermal plasma (NTP) technologies. These plasmas are useful for generating highly reactive species (e.g., free radicals) which readily decompose entrained pollutants in atmospheric-pressure gas streams. Such plasmas can generate both oxidative and reductive radicals - showing promise for treating a wide variety of pollutants, in some cases simultaneously decomposing multiple species. In this chapter, we will discuss the removal of gas-phase volatile organic compounds (VOCs) by two types of electric-discharge-driven NTPs: dielectric-barrier (silent) discharges and pulsed corona discharges. These two types of discharges are easily operated at atmospheric pressure or above, thereby having a high process throughput compared to low-pressure NTPs. Our main discussion topics are example applications of the technology, representative plasma reactors, reactive species generation, basic decomposition chemistry, typical experimental results which illustrate specific energy requirements for the decomposition of example pollutants, simple analytical removal-scaling models, and decomposition energy cost and optimization considerations. Historically, NTPs have also been applied to the removal of oxides of sulfur (SO_x) and nitrogen (NO_x) by both energetic electron-beam and electric-discharge NTP reactors. Those topics will not be treated in this chapter; for more information on de-SO_x/de-NO_x and electron-beam reactors, the reader is referred to the large body of existing literature on these subjects.

Chapter 10: Removal of Volatile Organic Compounds (VOCs) by Atmospheric-Pressure Dielectric-Barrier and Pulsed-Corona Electrical Discharges

Outline

10.1 Introduction

10.1.1 Background of Dielectric-Barrier and Pulsed-Corona Discharges for Environmental Applications

In the past decade, interest in non-thermal plasmas (NTPs) has grown considerably because of their applications to pollution control and hazardous waste treatment. In many cases this interest has been stimulated by a heightened concern over the pollution of our environment and more stringent environmental regulations (e.g., in the U.S, the Clean Air Act Amendments of 1990). NTPs, which generate highly reactive species such as free radicals, show particular promise for the treatment of gas-phase hazardous and toxic pollutants (e.g., volatile hydrocarbons and halocarbons and oxides of nitrogen and sulfur) because the reaction rates of free radicals with many compounds can be orders of magnitude larger than strong oxidizers like O_3 or H_2O_2.

A *non-thermal plasma* (also called non-equilibrium plasma) is characterized by electrons which are not in thermal equilibrium with the other gas species. The electrons are *hot* (~ few - 10s eV temperature), while the ions and neutral gas species are *cold* (near-ambient temperature). Such plasmas are good sources of highly reactive oxidative and reductive species, e.g., $O(^3P)$, OH, N, H, NH, CH, CH_3, HO_2, O_3, O_2 ($^1\Delta$), and plasma electrons. Because radical-attack reaction rate constants are very large for many chemical species, entrained pollutants are readily decomposed by NTPs. Using these reactive species, one can direct electrical energy into favorable gas chemistry through energetic electrons, rather than using the energy to heat the gas. NTPs are commonly created by an electrical discharge in a gas or the injection of an energetic electron beam into a gas [10.1]. Secondary plasma electrons, with a distribution of electron energies defined by an average electron energy (or electron temperature), are created by either method.

The electric-discharge-driven NTP-initiation of chemical reactions has a history of nearly one and one-half centuries. As exemplified by the generation of ozone in a dielectric barrier discharge by von Siemens [10.2], reactions of benzene in a corona discharge by Bertholot [10.3], and the work of Glockler and Lind [10.4]. Four useful reviews on the use of NTPs for bulk-volume plasma chemical processing are Eliasson and Kogelschatz 1991 [10.5], which primarily concentrates on the synthesis of ozone with silent electrical discharges - but briefly deals with other applications (flue-gas and hazardous-waste treatment) as well; Kogelschatz et al 1997 [10.6], which covers the silent-discharge applications of ozone synthesis, excimer lamps, plasma displays, CO_2 lasers, pollution control, surface modification, and greenhouse gas recycling; Chang et al 1991 [10.7], which reviews various NTP reactors, plasma-processing chemistry, and pollution-control applications; and Rosocha & Korzekwa 1999 [10.8], which covers non-thermal plasma destruction of pollutants in the context of an Advanced Oxidation Technology (AOT).

The history of treating hazardous and/or toxic chemicals with NTPs goes back over twenty years to military applications for destroying toxic chemical warfare agents with electric discharge reactors and civilian applications for treating flue gases (SO_x and NO_x) from electric power plants and other installations (e.g., steel mills) with electron beams.

The military applications focused on the removal of highly toxic chemical warfare agents from contaminated ambient-pressure air streams to produce breathable air streams (Tevault 1993 [10.9]). The first published account of the use of NTPs for decomposing chemical warfare agents involved the treatment of the surrogate agents dimethyl methylphosphonate (DMMP) and diisopropyl methylphosphonate (DIMP) with microwave-generated plasmas (Bailin et al. 1975

[10.10]). In the next decade, silent electrical discharges (dielectric-barrier discharges) were studied for this application by other researchers and results published on reactor modeling (Mukkavilli 1988 [10.11]) and on experiments with test compounds such as organophosphates (Clothiaux et al. 1984 [10.12]), methane (Fraser et al. 1985 [10.13], Tevault 1985 [10.14]), DMMP and trimethyl phosphate (Fraser et al. 1985 [10.15]), formaldehyde (Neely 1985 [10.16]), and hydrogen cyanide (Fraser et al. 1986 [10.17]). Because the military-directed systems did not demonstrate the ability to produce byproduct-free breathable air, interest in decomposing such chemicals with NTPs waned in the late 1980s.

The first civilian applications of NTPs for pollution control were focused on the removal of oxides of nitrogen and sulfur (NO_x, SO_x) with electron-beam reactors. The scrubbing of flue gases with electron-beam systems was initiated in 1970 in Japan by the Ebara Corporation; a history of e-beam flue-gas abatement can be found in Frank & Hirano 1993 [10.18]. A study on the electron-beam-initiated decomposition of an organic compound (vinyl chloride) was published in the early 1980s by Slater & Douglas-Hamilton 1981 [10.19] and, more recently, extensive work on e-beam treatment of VOCs has been done by the group at Karlsruhe (Paur 1993 [10.20]). Unfortunately, for the early scale-up demonstrations, a lack of commercial acceptance comparable to conventional systems contributed to a loss of interest in the technology. This interest seems to have been renewed recently, as evidenced by the construction and operation of large-scale facilities in Europe (Chmielewski et al. 1995 [10.21]).

The removal of SO_x and NO_x from gaseous media was also investigated at laboratory scale using electrical-discharge reactors (pulsed corona) in the 1980s - with pioneering experimental work performed for NO_x by Masuda 1988 [10.22], Masuda & Nakao 1990 [10.23] and for SO_x by Mizuno et al. 1986 [10.24]; and modeling work on streamer dynamics and radical yields was performed by Gallimberti 1988 [10.25]. Following these basic investigations, scale-up of the pulsed corona process for flue gases emitted from a coal-burning electrical power plant was carried out at pilot-plant and demonstration levels (Dinelli et al 1990 [10.26], Civitano et al 1993 [10.27]). Further modeling works on streamers and plasma-chemical reaction kinetics have since been carried out. For example, modeling of streamer morphology and dynamics is discussed by Vitello et al 1993 [10.28], Wang and Kunhardt 1990 [10.29], and Babeava & Nadis 1996 [10.30]; kinetic modeling of silent discharges has been done by Evans et al [10.31] for VOC removal and pulsed corona kinetics has been carried out by Lowke and Morrow 1995 [10.32] for SO_X and NO_x removal, and the simulation of streamers coupled with kinetic modeling has been performed by Li et al 1995 [10.33] for flue-gas treatment (SO_2 removal).

Further interest in NTP technology for destroying chemical pollutants arose in the late 1980s and early 1990s from greater concerns about toxic substances entering and spreading through the environment and the need to meet increasingly-stringent regulations on pollution. The earlier work on the destruction of nerve gases and flue gas cleanup has expanded to include many hydrocarbon and halocarbon compounds, typically at the laboratory and small pilot-scale levels using pulsed corona (Chang et al. 1991 [10.7], Grothaus et al 1993 [10.34]; [10.1]; Penetrante et al 1995 [10.35], 1996 [10.36], 1997 [10.37]; Hsiao et al 1995 [10.38]; Korzekwa et al. 1997 [10.39]; Puchkarev and Gundersen 1997 [10.40]; Smulders et al 1998 [10.41]), silent discharges (Neely 1993 [10.42], Storch & Kushner 1993 [10.43]; Rosocha et al 1993 [10.44]; Rosocha 1997 [10.45]; Coogan et al 1993 [10.46]; Evans et al 1993 [10.31]; Falkenstein 1997 [10.47]; Krasnoperov et al 1997 [10.48]; Snyder & Anderson 1999 [10.49]), electrified packed-beds (Virden et al. 1992 [10.50]; Nunez et al.1993 [10.51]), and electron beams (Paur 1993 [10.20];

Penetrante et al 1995 [10.35-10.37]; Bromberg et al 1993 [10.52]; Koch et al 1993 [10.53]; Matthews et al 1993 [10.54]; Vitale et al 1996 [10.55]).

This chapter will review of the subject of pollutant decomposition by atmospheric-pressure electric-discharge-excited silent discharge (dielectric barrier) and pulsed corona NTP reactors, which serve as tools for driving free-radical-initiated decomposition reactions. Our main discussion topics are example applications of the technology, representative plasma reactors, reactive species generation, basic decomposition chemistry, typical experimental results which illustrate specific energy requirements for the decomposition of example pollutants, simple analytical removal-scaling models, and decomposition energy cost and optimization considerations.. Our emphasis is on the two electric-discharge NTP reactors mentioned above; electron-beam reactors have been briefly discussed but the reader is referred elsewhere for more details on that subject ([10.1], [10.18], [10.19], [10.20], [10.35-10.37], [10.52-10.55], Cohn 1997 [10.56]).

10.1.2 Electrical Discharge Physics and Plasma Chemistry

Background

Silent discharge (dielectric barrier) and pulsed corona reactors both create transient electrical-discharge streamers in a gas. The streamer is the source of energetic electrons and other active species. A relatively high electric field (determined by the reactor geometry, gas composition, gas pressure, and gas temperature) is required to cause electrical breakdown in the gas. The necessary breakdown voltage is supplied by a drive circuit connected to the reactor. In corona, a non-homogeneous electric field is used to stabilize the discharge via the buildup of space charge around the corona wire (corona streamer dynamics are controlled by localized space-charge waves) and to prevent thermal arc formation. Silent discharges use charge buildup on a capacitive barrier to achieve a similar end result. Two similar, but not illustrated, reactors are the electrified packed bed (Mizuno & Ito 1990 [10.57]; [10.50, 10.51]; Yamamoto et al 1993 [10.58]; Lermer et al 1995 [10.59]; Tonkyn et al 1996 [10.60]) and the surface-discharge reactor (Masuda 1993 [10.61] and Puchkarev et al 1994 [10.62]) which are closely related to a barrier discharge in that streamers are created between dielectric pellets or across dielectric surfaces.

In general, the streamers created in all types of atmospheric-pressure electric discharges can be thought of as cylindrical current filaments with typical radius ~ 100 μm. They are transient discharges (e.g., lasting only a few nanoseconds for oxygen or air), fed by ionization and detachment and then arrested when the electric field is reduced to the point where electron attachment becomes dominant. For streamers in pure oxygen and air, the average electron energy and electron density are $T_e \sim 3\text{-}5$ eV, $[e] \sim 10^{14}/cm^3$, while a typical breakdown reduced electric field strength in the gas is $E/N \sim 100 - 200$ Td. Multiple streamers typically give accumulated plasma energy loadings of 10s - 1,000s J/L atm. For further descriptions of streamers and gas-discharge physics, the reader is referred to the pioneering streamer (or "Kanal Theory") work of Raether 1964 [10.63], the book by Raizer 1991 [10.64] and a recent book on pulsed gas breakdown by Korolev and Mesyats 1998 [10.65].

10.2 Representative Dielectric-Barrier and Pulsed-Corona Reactors

10.2.1 Overview

Figure 10.1 shows simple schematic diagrams of silent discharge and pulsed corona reactors for gas-phase pollutant processing ([10.1], [10.20], [10.22], [10.23], [10.34], [10.44, 10.45], [10.57]). In these reactors, a high voltage is applied across the electrodes in the gas. The energetic plasma electrons created in the ensuing electrical discharge create active species (free radicals and secondary electrons) that attack pollutants entrained in the process gas.

INSERT FIGURE 10.1 NEAR HERE

10.2.2 Plasma Reactor Excitation Specific Power and Energy

The free radicals and other active species produced in a non-thermal plasma reactor are produced by the electrical power and energy which excites the electrical-discharge volume. To understand the performance of and scale-up of NTP reactors, it is necessary to understand how the excitation power and energy relates to the properties of the electrical discharge.

Pulsed corona reactors (PCRs) and dielectric barrier (silent discharge plasma - SDP) reactors both employ similar electrical-discharge streamer mechanisms, which results in similar electron temperatures (and active-species production efficiencies) for both devices. However, their practical specific powers and energies (power and energy per unit plasma volume) are vastly different, as shown below. The specific excitation power for an SDP reactor has been previously derived [10.45] and can be expressed as

$$\bar{P} = 2fa\sigma\bar{E}_{\mu}, \tag{10.1}$$

where $\bar{P}$ is the specific power, f is the frequency of the ac voltage supplied to the reactor, σ is the number of microdischarge streamers per unit area, and $\bar{E}_{\mu}$ is the specific energy per microdischarge.

An analogous expression can be derived for a wire-cylinder PCR

$$\bar{P} = f\bar{E}_{\lambda}/\pi R^2, \tag{10.2}$$

where $\bar{E}_{\lambda}$ is the energy deposited in the PCR per unit length, R is the cylinder radius, and the other variables are the same as those for the SDP reactor.

The specific energy $\bar{E}$ is related to the specific power $\bar{P}$ and the gas residence time in the active volume of the reactor τ_r by the expression

$$\bar{E} = \bar{P}\,\tau_r. \tag{10.3}$$

Figure 10.2 shows a plot of specific energy versus gas residence time for typical PCR (solid line) and SDP (dashed line) devices. The specific energy is the product of specific plasma power and residence time. For two reactors with similar active volumes, the higher the specific power, the shorter the required residence time for a given degree of removal (and the higher the possible gas flow rate).

INSERT FIGURE 10.2 NEAR HERE

SDP reactors can easily achieve specific powers in excess of 1 W/cm^3, while PCRs typically achieve specific powers of about two orders of magnitude less. A recent investigation on electrical pulse generators for practical PCRs by Rea et al 1995 [10.66] has demonstrated an optimal injected energy of 4.8 mJ/cm which, for their 20-cm diameter active-volume reactor, translates into a specific power of 15.3 mW/cm^3 (assuming an achievable pulse repetition frequency of 1 kHz - an optimistic value, considering the present state-of-the-art in practical pulsed power switchgear). Creyghton et al [10.67] have shown similar linear energy density values of 3.5 mJ/cm, with pulsed corona voltage rise times of 40 ns.

In PCR and SDP electrical-discharge reactors, the specific energy required for one e-fold (63%) removal of flue gases such as NO_x and SO_x is relatively modest (about 50 or 60 J/liter in air), approximately bordering the bottom of the shaded portion of Figure 10.2. The PCR specific energy line is near this region, so a PCR can produce flue-gas removal with reasonable residence times (or gas flow rates). In contrast, the shaded portion of Figure 10.2 approximates the specific energy range required for one e-fold removal of many VOCs in air by electrical-discharge reactors (e.g., 75 - 200 J/L for toluene and 400 - 1700 J/L for methylene chloride). From the figure, one observes that a PCR must have a very large residence time compared to an SDP reactor (or be scaled to a much larger active volume) to produce degree of removal comparable to SDP reactors. Because of the high specific power of an SDP reactor, it can process energy-demanding gases at reasonably high gas flow rates and achieve relatively high degrees of removal, all with more compact reactors.

If one can increase the active-species production efficiencies, the specific energy for a given degree of removal is reduced. This well illustrated in electron-beam reactors where more energetic electrons produce radicals at higher yields. There is evidence that some improvement in radical yields is possible in electrical-discharge reactors by applying very short rise time electrical drive pulses [10.40]. Because electrical discharge reactors are presently thought to be less expensive and less maintenance-intensive than electron-beam reactors, such improvements are attractive for improving the overall systems perspective for discharge reactors.

10.3 Active Species Production and Illustrative Decomposition Chemistry

In the decomposition process, plasma physics and plasma chemistry are interconnected: understanding this coupling is essential to being able to gain an understanding of and optimize the overall pollution-control process. The electrical discharge creates the plasma which, in turn, generates active species in the pollutant-containing gas. The active species then react with and decompose the chemical pollutants. In a simple view, the active-species production and pollutant-decomposition processes can described by a net energy efficiency, where the formation and utilization of active species is separated, according to the following equation [10.44, 10.45]:

$$\eta_{net} = \sum_i \eta_{f,i}\, \eta_{u,i} \,, \tag{10.4}$$

where η_{net} is the net number of pollutant molecules decomposed per unit deposited energy, $\eta_{f,i}$ is the formation efficiency (yield) of the i^{th} active species, and $\eta_{u,i}$ is the utilization efficiency (probability of interacting with the target pollutant) for the i^{th} species. In electric discharges $\eta_{f,i}$

mostly depends on the fast electron and excited-state quenching processes, while $\eta_{u,i}$ mainly depends on the active-species, pollutant-interaction reaction chemistry.

Below, for an air-like gas, we briefly discuss active species (i.e., radical) generation and the decomposition chemistry for two example VOC pollutants: the chlorocarbons trichloroethylene (C_2HCl_3, abbreviated TCE) and carbon tetrachloride (CCl_4).

10.3.1 Active Species (Free-Radical) Production

Active species can be formed in a variety of ways in non-thermal plasmas. Table 10.1 shows the main processes for an air-like carrier gas. Electron collisional dissociation or excitation of background gas molecules are the main mechanisms for producing active species. Additionally, negative ions can also lead to active species formation. Because the negative ion reactions represent additional energy pathways, negative ion reactions can change the distribution function and the electron density and, therefore, affect the yields of active species. This is especially true when comparing the cases of dry air and humid air (Morgan et al 1995 [10.68]), where the electron density is significantly less in humid air for a given value of E/N.

INSERT TABLE 10.1 NEAR HERE

In chlorine-compound-containing mixtures, Cl and ClO radicals are also produced from reactions of radicals and other gas species with the entrained pollutants. These can further participate in decomposition chain reactions, which improves the overall decomposition efficacy (e.g., see Evans et al [10.31], Falkenstein [10.47], and Vitale et al [10.69]). The yield of a particular radical species (i.e., the number of radicals produced per unit deposited plasma energy) will depend on factors such as the gas composition, the gas pressure, and the average electron temperature. The Yield is frequently described by the G-value (species per 100 eV deposited energy), which is a function of an effective rate constant for radical generation k_{rad} (e.g., the dissociation rate constant for dissociating O_2 molecules into O-atoms), the electron drift velocity v_d, and the reduced electric field strength E/N

$$G = f\left(\frac{k_{rad}}{v_d \frac{E}{N}}\right) . \qquad (10.5)$$

The rate constant k_{rad} and the drift velocity v_d also depend on the reduced field E/N (electron temperature), so the G-value essentially depends on E/N and the plasma-chemical kinetics leading to the generation of active species [10.35, 10.44, 10.45].

Consider humid, atmospheric pressure air; here the yields of $O(^3P)$, OH, and N radicals in typical electric-discharge reactors are of order 10, 1, and 1 per 100 eV of deposited energy, respectively [10.44, 10.45]. For electron-beam reactors, the $O(^3P)$ yield is about one-third less, the yield of OH is roughly twice as large, and the yield of N is nearly 10 times larger than in discharge reactors [10.1, 10.35]. Usually, at near-atmospheric pressure, pollutants in the concentration range of interest (100s to 1000s ppm) do not affect the electron distribution function or the associated electron temperatures and radical yields.

10.3.2 Basic Decomposition Chemistry

The plasma-generated active species (radicals and secondary electrons) are the initiators of pollutant-decomposition reactions [10.1]. Two major decomposition channels for a gas-phase chemical pollutant X are direct electron impact and chemical (radical-promoted) attack:

$$e + X \rightarrow \text{products} \qquad \text{and} \qquad O, OH + X \rightarrow \text{products.}$$

The first path is expected to dominate at large contaminant concentrations (when a higher energy fraction is absorbed by the pollutant) or when the dissociative attachment cross section is large, while the second should dominate at smaller concentrations.

Additionally, some molecules may decompose by ion-molecule reactions as demonstrated by Penetrante et al. 1997 [10.70] for the dissociative charge exchange decomposition of methanol

$$N_2^+ + CH_3OH \rightarrow CH_3^+ + OH + N_2$$

and also postulated by Krasnoperov et al [10.48] and Nunez et al [10.51] for other hydrocarbons.

Many VOCs, will often undergo a series of more complicated reactions before the final products result. The decomposition of a chlorocarbon like trichloroethylene is dominated by free-radical reactions at the relatively high E/N of electric discharges (Evans et al [10.31], Falkenstein [10.47], Penetrante et al [10.37], Hsiao et al [10.38]).

$$O(^3P) \text{ or } OH + C_2HCl_3 \rightarrow CO_2 + HCl + Cl_2 + COCl_2 + \ldots.$$

However, strong electron attachers (e.g.,CCl_4) are preferentially decomposed by dissociative electron attachment at low E/N (Storch et al. 1991 [10.71]; Penetrante et al 1995 [10.35]).

$$e + CCl_4 \rightarrow CCl_3 + Cl^-$$
$$CCl_3 + O_2 \rightarrow COCl_2 + Cl + ClO\,.$$

In this section, we have only included a very simplified set of the basic decomposition reactions. Aerosol formation (from ion-neutral clustering) can lead to additional reactions on the surface of the particles. This can, in some cases, increase the effective removal of pollutants in the gas or a change in the final products (Chang et al [10.7]).

The molecular structure of a compound can also affect the energy required for decomposition (Neely et al [10.42], Futamura et al 1997 [10.72]) For example, the difference in the degree of difficulty of free-radical-induced decomposition of TCE versus trichloroethane ($C_2H_3Cl_3$, abbreviated TCA) can be explained by the structures of the respective molecules and the point of attack of a radical on the molecule. For TCE, its two carbon atoms have a double bond, with one Cl and one H atom bound to one carbon and two Cl atoms bound to the other. For the haloalkenes, including TCE, the main point of attack of an O-radical or OH-radical is the double bond of carbon (Vitale et al [10.69]). This results in the cleavage of the double bond to a single bond and the bonding of the O or OH-radical to the least-chlorinated carbon atom. In the presence of oxygen, the radical formed from this process can then further decompose or lead to the formation of other radicals which tend to attack TCE. For TCA, its two carbon atoms have a single bond, with two H atoms and one Cl atom bound to one carbon and two Cl atoms and one H atom bound to the other carbon. The single bond is not receptive to attack by Cl radicals; therefore, TCA is much harder to decompose than TCE.

Decomposition is not necessarily complete treatment - the goal is to produce less-toxic or more easily-managed final products. Byproducts must also be considered (e.g., $COCl_2$ is toxic but is easily removed by reactions with water and HCl can be easily neutralized by a base solution) In laboratory studies, the degree of decomposition and treatment byproducts are measured with an instrument like a gas chromatograph - mass spectrometer.

The detailed plasma-initiated removal chemistry of a particular compound or mixture of compounds can be quite complicated and will not be addressed here. This topic has been addressed at length by various authors, so for more information, the reader is referred to the literature (e.g., Evans et al [10.31], Falkenstein [10.47], Penetrante et al 1997 [10.73, 10.74], and Vitale et al [10.55, 10.69]).

10.3.3 Example Decomposition Plots

In many non-thermal plasma devices (like ozonizers, gas lasers, etc.,), a key process parameter is the specific energy (plasma energy density) deposited in the gas. This is also true for the decomposition of a pollutant in an NTP reactor. Experiments with various reactors have shown that the degree of removal of a particular contaminant depends on the applied plasma energy density $\bar{E}$ and a characteristic energy-density parameter (which we call β) which is related to the target compound, the carrier gas, and the reduced electric field E/N for the reactor [10.1, 10.35, 10.44, 10.45]. The energy density is usually expressed in J/standard liter (J/L).

In general, the degree of removal of a particular contaminant species can be rather accurately approximated as an exponential function of the parameters $\bar{E}$ and β [10.44, 10.46]

$$[X] = [X]_0 \exp(-\bar{E}/\beta), \tag{10.6}$$

where $[X]_0$ is the initial pollutant concentration, [X] is the pollutant concentration after depositing a plasma specific energy of $\bar{E}$ into the treated gas, and β is a specific energy characteristic of a given compound, which reduces the concentration by 1/e (one e-fold reduction).

The ratio $[X]/[X]_0$ is our definition of a degree of removal - the ratio gets smaller as more pollutant is removed. The fraction (or %) of pollutant removed is $1 - ([X]/[X]_0)$ (or times 100 for removal in %). In much of the literature in this field, the fractional removal $1 - ([X]/[X]_0)$ is called the "removal efficiency". However, we do not promote the use of the term in that manner. Instead, we think of efficiency as the energy efficiency of removing a pollutant.

$\bar{E}$, the accumulated plasma energy density loading, gives quite useful information, because it is a key parameter which determines how much pollutant is removed and the energy efficiency of removing it (as demonstrated by the presented examples and the simple removal model, both discussed further below). The specific energy is useful in that it is *explicitly independent* of the particular reactor employed and the gas residence time. $\bar{E}$ is the analog of dose in radiolytic treatment, where similar removal relationships apply. Therefore, to simplify matters, we can think of the reactor as a 'black box' which processes a concentration $[X]_0$ into a concentration [X] under the influence of a plasma specific energy $\bar{E}$.

Such a relationship is representative of chemical-kinetic rate equations that are first order in the concentration of the contaminant. In the next section, we will show that simple, first-order kinetics models can be used to derive a pollutant-removal function whose form is representative of example decomposition plots taken from the literature and shown in Figures 10.3a-10.3d below.

INSERT FIGURES 10.3a-10.3d NEAR HERE

10.4 Typical VOC-Removal Experiments and Results

At Los Alamos, we have carried out experiments on the decomposition of several hydrocarbons, halocarbons, and nitric oxide using pulsed corona and dielectric-barrier discharges at ambient pressure (i.e., ~ 580-600 torr). In this section, we will discuss tests on two representative VOCs, namely TCE and methyl ethyl-ketone (MEK) in dry air. Other laboratory-scale experiments related to our work at Los Alamos are discussed or referenced elsewhere (Rosocha et al [10.44, 10.45]; Korzekwa et al. [10.39]; Coogan et al. [10.46]; Falkenstein [10.47]; Snyder & Anderson [10.49]; Coogan & Jassal 1997 [10.76]). Many other experiments are described in reference [10.1], the others cited above, and in the literature.

10. 4.1 Apparatus and experimental Methods

Our pulsed corona reactor tube was constructed using a stainless steel corona wire with a diameter of 500 μm and stainless steel tubing with an inner diameter of 2.5 cm as the outer conductor. The length of the tube was 90 cm. A high-voltage alumina feedthrough was employed at one end to apply the electrical pulse (positive polarity) to the wire and another alumina insulator was used to support the opposite end of the wire. The gas flow was introduced into the tube through gas fittings at the gas manifolds on each end. This reactor design could be used up to temperatures of 700 C.

An electrical schematic diagram of the pulsed corona apparatus is shown in Figure 10.4. A constant current power supply (EMI model 500-40KV-POS) is used to repetitively charge a storage capacitor, C_{sp}, with a repetition frequency set by the control module. When the breakdown voltage of the coaxial, self-breaking, hydrogen-filled spark gap is reached, a high voltage pulse is delivered to the reactor tube capacitance, C_{pcr}, through the stray inductance, L_s. When the corona inception voltage is reached in the reactor tube, multiple simultaneous streamer-discharges (represented by a time varying resistance R_d) are produced in the tube.

INSERT FIGURE 10.4 NEAR HERE

A coaxial capacitive voltage divider, V_{pcr}, was constructed at the input to the tube. The voltage probe had a sensitivity of 2.5×10^{-4} V/V and was capable of measuring nanosecond rise time pulses with pulse widths less than 150 ns. The pulsed corona current was measured using a current viewing resistor, R_{cvr}, which was also connected at the reactor input. This probe was capable of measuring nanosecond rise time pulses with a sensitivity of 20 A/V. The power dissipated in the discharge was measured using these probes. A feedback signal from the current probe (signal to indicate the switching of the spark gap) was sent to the control module to inhibit the power supply. For C_{sp} = 126 pF, L_s = 400 nH, and C_{pcr} = 25 pF, the waveforms in Figure 10.5 were obtained showing the voltage and current of a typical corona pulse in dry air at room temperature. The energy per pulse E_0 dissipated in the discharge was approximately 60 mJ. $\bar{E}$ is then calculated using the expression $\bar{E} = E_0 f_r / Q$, where f_r is the pulse repetition frequency and Q is the gas flow rate in L/s. The system could be operated at a repetition frequency greater than 1 kHz with a peak output voltage of up to 30 kV.

The circuit representation in Figure 10.4 of the pulsed corona apparatus includes (in part) a series resonant circuit. When the switch closes the energy in the storage capacitance (C_{SP}) is resonantly transferred to the corona tube capacitance (C_{PCR}) through the stray inductance (L_S). The displacement current associated with this resonant energy transfer is apparent from the high-frequency oscillation which is superimposed on the overdamped corona current pulse (or discharge current). By multiplying the current and voltage waveforms and integrating over the pulse width, the energy per pulse dissipated in the discharge can be calculated. Using this method the reactive power associated with the displacement current will integrate to zero leaving only the real dissipated power.

INSERT FIGURE 10.5 NEAR HERE

A schematic diagram of the ac-driven dielectric-barrier discharge system is shown in Figure 10.6. A variable frequency, 3-kW, ac power supply (Elgar model 3001-165A) was used to drive a high-voltage 50:1 step up transformer (Stangenes Model SI-8020) which supplied power to the dielectric-barrier discharge cell. The operating frequency was 1.2 kHz, with variable discharge powers up to 350 W. The discharge cell was constructed in a flat-plate geometry using two 0.3 cm x 38 cm x 70 cm Pyrex plates with a gap spacing of 3.5 mm and an active discharge area of 1800 cm^2. Two aluminum electrode plates were pressed to each side of the cell. A charge measuring capacitor, C_Q, was placed in the circuit between the low voltage plate and ground. The charge through the cell is proportional to the voltage measured across C_Q (Q_{CELL} in Figure 10.6). The output of the high-voltage transformer was connected to ground and the high-voltage electrode plate. A high-voltage probe (Tektronix model P6015A) was used to measure the voltage across the cell, V_{CELL}. Typical waveforms of the voltage and charge versus time are shown in Figure 10.7a. Using the method invented by Manley 1943 [10.77], the energy per cycle delivered to the discharge was obtained by plotting the charge driven through the cell versus the voltage across the cell for one cycle then calculating the area of the resulting parallelogram, shown in Figure 10.7b. The power dissipated in the discharge, in Watts P, was then found by multiplying the energy per cycle by the operating frequency. The energy density is computed using the relationship $\bar{E} = P/Q$.

INSERT FIGURES 10.6 & 10.7a & 10.7b NEAR HERE

The chemical diagnostics setup is shown in Figure 10.8. For the TCE and MEK measurements, a gas bottle was filled to a high pressure with a mixture of dry air and the desired VOC concentration. A mass flow controller was used to set the flow through the discharge tube or cell before entering the vent. For benchtop work, typical gas flow rates for the pulsed corona reactor are 0.25-5 L/min and 10-20 L/min for the silent discharge reactor. These correspond to gas residence times in the reactor of 5.3-106 s for the pulsed corona setup and 0.93-1.86 s for the silent discharge setup. Two methods were used to measure the decrease in VOC concentration, 1) a gas-chromatograph/mass-spectrometer, GC/MS, (HP model 5890 GC and HP model 5972 MS) was connected directly to the output line of the discharge volume and 2) a gas-tight syringe was used to extract a sample at a known volume from the gas output line which was then injected into a gas chromatograph with a sample concentrator (Varian model Star 3400CX GC and OI Corp. model 4460A sample concentrator). The data for the ac-driven dielectric-barrier discharge

was obtained using the GC/MS and the data for the pulsed corona discharge was obtained using the GC with a sample concentrator.

INSERT FIGURE 10.8 NEAR HERE

10.4.2 Experimental Results

The removal of two VOCs, TCE and MEK, in dry air has been measured using the two different discharge reactors. The removal fraction is defined as $[X]/[X]_o$, where $[X]_o$ is the initial concentration and [X] is the final concentration in units of ppmv. The removal fraction (or degree of removal) is plotted as a function of plasma energy deposited into the gas or specific energy, $\bar{E}$ (or, equivalently deposited power divided by gas flow rate P/Q).

Comparison of Silent Discharge and Pulsed Corona Reactor Performance

The first measurements were made using the VOCs to compare the pulsed corona and ac-driven dielectric-barrier discharges at room temperature. Figure 10.9 shows the removal fraction versus $\bar{E}$ for 200 ppm of TCE, where there is no noticeable difference in the removal efficiency for energy densities up to 400 J/L between these two types of discharges. A double-exponential curve fit is also plotted which shows a slight divergence from a single-exponential fit (a straight line), likely indicating reactions other than first order at the higher energy densities. A double-exponential curve fit applies to the VOC-removal data presented here. A similar plot for 1000 ppm of MEK is shown in Figure 10.10, where for energy densities up to 1500 J/L, there is no distinguishable difference in the degree of removal. However, for higher energy densities there is a slight difference which can be attributed to a difference in gas temperature in the PCR, which will be discussed in the next section.

INSERT FIGURES 10.9 & 10.10 NEAR HERE

Gas Temperature Effects

Depending on the compound to be treated and the reaction chemistry, the removal fraction can be greatly affected by temperature. The temperature dependence of the reaction kinetics has the form $k = A \exp(-T_A/T)$, where k is the rate constant in units of cm^3/molecule-s, A is the pre-exponential factor with the same units as k, and T_A is the activation energy in units of temperature (K). For reactions with $O(^3P)$, the values of T_A are 1000 K and 1300 K for TCE and MEK respectively (Westley et al 1994 [10.78], Ott et al 1987 [10.79]). To achieve the high energy densities in Figure 10.10, the pulsed corona tube was operated at powers up to 30 W, which resulted in a temperature increase of up to 60 C. It is plausible that the slight increase in the removal fraction of MEK in Figure 10.10 at energy densities higher than 1500 J/L is attributed to this increase in gas temperature. A temperature rise was not observed in the measurements for TCE using the pulsed corona discharge because the powers necessary to achieve energy densities up to 400 J/L were very low (a few watts). The temperature in the ac-driven dielectric-barrier discharge always remained near room temperature.

It is well known that the breakdown voltage (V_{BR}) of a gas is temperature dependent. From Alston [10.80], an empirical functional form for this temperature dependence is given, where V_{BR} decreases with an increase in temperature. However, the gas density is also temperature dependent (inversely proportional), such that, when the E/N at breakdown (E_{BR}/N) is

determined using these functional forms, the value of E_{BR}/N increases with temperature. Because the relationship between the E/N value at breakdown and the maximum E/N value generated in the tip of the streamer (in a pulsed corona discharge for example) is not well known, one can only speculate on the effects of the increase in E_{BR}/N on the generation of radical species.

10.4.3 Discussion of Results

The breakdown voltage in the pulsed corona discharge is much higher than in a low-frequency ac-driven dielectric barrier discharge. The minimum voltage to produce a discharge in the pulsed corona tube at ambient pressure (about 580 torr) was 12 kV for this wire and tube size, which, if only the geometry is taken in consideration, produces an electric field of 120 kV/cm at the wire surface. The breakdown voltage in the ac-driven dielectric barrier cell at ambient pressure was 7 kV at 1.2 kHz with a 3.5-mm air gap, which gives an electric field of 20 kV/cm. With such a large difference in breakdown electric field, it is reasonable to expect a difference in removal fractions between the ac-driven and pulsed corona discharges. However, as seen in the VOC data, there was no difference in removal fractions between the different types of discharges at room temperature. To explain this, the reaction pathways leading to the destruction of these compounds must be investigated. For TCE and MEK in air it is well known that the initial chemical reaction is with the $O(^3P)$ radical produced in the discharge (Westley et al [10.78]). In that case, the production of $O(^3P)$ as a function of the reduced electric field strength E/N (which is also a measure of the average electron energy in the discharge) is important.

As observed in Equation 5, radical-production G-values depend on E/N. The values of the breakdown E/N derived from the breakdown electric fields calculated above are 80 Td for the ac-driven dielectric-barrier discharge and approximately 500 Td for the pulsed positive corona discharge at room temperature and pressure. The two possible explanations for the same removal efficiencies at different breakdown fields are: 1) the radical production happens to be approximately the same for the 80 Td discharge and the 500 Td discharge ($O(^3P)$-radical production G-values at first rise with increasing E/N and then fall off at higher E/N (Rosocha et al [10.44, 10.45]; Li et al 1995 [10.33]), or 2) the observed removal fractions (which correspond to radical formation efficiencies) suggest equivalent average conditions, where the radical formation depends on an average value of E/N (or electron energy), which may be very similar for the low-frequency and pulsed discharges.

10.5 Pollutant-Removal Relationships

10.5.1 Simple Reaction-Kinetics Model and Derivation of Removal Equations

Recent work on comparing pollutant decomposition by different aqueous-phase AOTs has shown that, even though the overall decomposition chemistry of a particular chemical species can be quite complicated, simple kinetic models can be used to describe the rate of radical-initiated decomposition of a target species (Bolton et al. 1996 [10.81]). Using an analogous method for a gas-phase NTP process, we will describe the decomposition of a pollutant X (in a carrier gas of species A and containing radical scavengers S_i) by the following simple chemical reactions and rate equations:

Chemical Reactions Rate Equations

$$e + A \rightarrow R\cdot + A' \qquad \frac{d[R\cdot]}{dt} = \frac{d[R\cdot]}{d\bar{E}} \cdot \frac{d\bar{E}}{dt} = G\bar{P} \ , \tag{10.7}$$

$$R\cdot + X \rightarrow \text{Products} \qquad \frac{d[X]}{dt} = -k[R\cdot][X] \ , \tag{10.8}$$

$$R\cdot + S_i \rightarrow \text{Products} \qquad \frac{d[R\cdot]}{dt} = -k_{S_i}[R\cdot][S_i] \ , \tag{10.9}$$

where [X] is the pollutant concentration, G is the production efficiency for radical species R·, $\bar{P}$ is the plasma power density, k is the radical-pollutant kinetic rate constant, $[S_i]$ is concentration of the i^{th} scavenger, and k_{Si} is the scavenging rate constant for the i^{th} species.

Because the rate of radical-pollutant attack is usually quite fast, it is reasonable to assume that the radical R· is consumed as quickly as it is produced; that is, a steady-state approximation for [R·] holds. Under this steady-state assumption, the net rate of change of R· is zero and can be expressed as

$$\frac{d[R\cdot]}{dt}(net) = G\bar{P} - k[R\cdot][X] - \sum_i k_{S_i}[R\cdot][S_i] = 0 \ . \tag{10.10}$$

Solving this equation for the steady-state concentration $[R\cdot]_{ss}$, inserting it into Equation 10.8, making the substitution $\bar{P} = d\bar{E}/dt$, and rearranging terms, one obtains the following generalized removal differential equation

$$\frac{k[X] + \sum_i k_{S_i}[S_i]}{k[X]} d[X] = -G d\bar{E} \ . \tag{10.11}$$

Integration of this equation with the limits $[X]_0 \rightarrow [X]$ and $0 \rightarrow \bar{E}$ gives the transcendental equation

$$\frac{[X]}{[X]_0} + \frac{\sum_i k_{S_i}[S_i]}{k\,[X]_0} \ln\frac{[X]}{[X]_0} - 1 = -\frac{G\bar{E}}{[X]_0} \ . \tag{10.12}$$

When the degree of removal is low; ie., when $[X]/[X]_0 \cong 1 + \ln([X]/[X]_0$, the following analytical solution (same as Equation 1) is obtained

$$[X]/[X]_0 = \exp(-\bar{E}/\beta) \ , \tag{10.13}$$

where

$$\beta = \frac{1}{G}\left([X]_0 + \frac{\sum_i k_{S_i}[S_i]}{k}\right) . \qquad (10.14)$$

When the rate of radical-pollutant attack k[X] is small compared to the rate of radical scavenging Σ_i k_{Si} $[S_i]$, the β-value and, hence the degree of removal $[X]/[X]_0$ shows no dependence on the initial concentration $[X]_0$. Similar relationships for the pollutant removal function and its concentration dependence have been derived for electron-beam reactors by Slater & Douglas-Hamilton [10.19] and Vitale et al [10.55], assuming that the scavengers are actually products of the initial radical-attack reaction (radical-inhibitor model); and for an electrified packed-bed reactor by Tonkyn et al 1996 [10.60], with similar assumptions but also taking active-species scavenging by the reactor substrate into account.

In Equation 10.13, $\bar{E}$ is the applied specific energy (or plasma power divided by gas flow rate, P/Q), and β is the e-fold energy density. Supplying one β to the reactor reduces the concentration by 1/e, 2β by $1/e^2$, and so on. When the β-value is independent of the initial concentration, a plot of the logarithmic degree of removal $-\ln([X]/[X]_0)$ versus $\bar{E}$, gives a straight line of slope 1/β. For other cases, the plot is not necessarily a straight line, so such a slope-determined β-value is only an approximation. When the β-value shows a stronger dependence on the initial pollutant concentration, the removal plot will consist of a family of curves.

Equation 10.13 does not necessarily apply in all cases. In general, one must numerically solve Equation 10.12 to obtain the actual removal functions. When the degree of removal is high, the removal plots can show considerable curvature, as observed by Slater & Douglas-Hamilton [10.19] and Vitale et al [10.55].

The β-value links the generation of radicals through gaseous electronics/plasma chemistry (G-values) with their utilization through the decomposition chemistry. As previously shown in Equation 10.5, the G-value is a function of an effective rate constant for radical generation k_{rad} (e.g., the dissociation rate constant for dissociating O_2 molecules into O-atoms), the electron drift velocity v_d, and the reduced electric field strength E/N. The rate constant k_{rad} and the drift velocity v_d also depend on the reduced field E/N (electron temperature), so the β-value essentially depends on E/N and the chemical kinetics [10.35, 10.44, 10.45].

10.5.2 Example Removal Plots for Special Cases

To show how this simple model predicts the form of the removal equation (as observed in the example decomposition plots presented earlier), we illustrate two examples below. In the first example, the rate of radical scavenging is much greater than the rate of radical attack; i.e., $k[X]_0 << \Sigma_i k_{Si} [S_i]$; in the second example, the opposite situation holds, i.e., $k[X]_0 >> \Sigma_i k_{Si} [S_i]$.

Figures 10.11a and 10.11b show the removal plots that correspond to these examples for representative values of the initial concentrations and specific plasma energies.

INSERT FIGURES 10.11a & 10.11b NEAR HERE

There is also a third example, the case in which radical-radical recombination dominates both scavenging and radical-pollutant attack, that is of interest. The removal equation for this case explicitly depends not only on the specific energy $\bar{E}$ but also on the gas residence time in the reactor τ_r. The removal equation in this case is derived by solving Equation 10.10 for $[R\cdot]_{ss}$ under

the assumptions that $\Sigma_i\ k_{Si}\ [S_i] >> k\ [X]_0$ and that the dominant scavenging pathway is recombination of the radicals, e.g., $[R\cdot] = [S]$, where S represents the primary scavenger.

Making these assumptions and solving Equation 10.10 for $[R\cdot]_{ss} = [R\cdot]$, we obtain

$$[R\cdot] = (G\bar{P}/k_s)^{1/2}. \tag{10.15}$$

Substituting this into Equation 10.8, one gets the expression

$$\frac{d[X]}{[X]} = -k\left(\frac{G\bar{P}}{k_S}\right)^{1/2} dt\ . \tag{10.16}$$

Integrating this equation with limits $[X]_0 \rightarrow [X]$, $0 \rightarrow \tau_r$ and making the substitution $\bar{E} = \bar{P}\,\tau_r$, we get the following removal equation

$$[X]/[X]_0 = \exp\{-k(G\bar{E}/k_s)^{1/2}\tau_r^{1/2}\}. \tag{10.17}$$

As an example of this case, consider a model situation for the compound methyl chloride (CH_3Cl) in an $Ar/O_2/H_2O$ gas mixture of composition 78/20/2. Such a mixture has a G-value of 7.5 for the generation of OH [10.44, 10.45]. CH_3Cl is attacked by OH radicals via the reaction

$$OH + CH_3Cl \rightarrow \text{Products}\ (k = 4.57 \times 10^{-14}\ cm^3/s\ [10.82]),$$

and the OH radicals are most strongly scavenged via the reaction

$$OH + OH + M \rightarrow H_2O_2 + M\ (k_s = 6.5 \times 10^{-34}\ cm^6/s\ [10.83]).$$

Assuming atmospheric pressure (gas density of 2.7×10^{19} molec/cm^3), substituting the rate constants k and k_s into Equation 10.17, and calculating the removal fraction $[X]/[X]_0$ over a range of $\bar{E}$ and τ_r values gives the example plot shown in Figure 10.12. Presently, we have no experimental data with which to compare this sample calculation. O-atoms also attack CH_3Cl. However the attack rate constant is much smaller than that for OH and the O-atoms are lost much more quickly to the formation of O_3, rather than radical-radical scavenging.

INSERT FIGURE 10.12 NEAR HERE

10.6 Energy Cost and Optimization

Optimizing the performance (degree of removal of the pollutant, decomposition products, energy consumption, etc.) of an NTP reactor is a complicated process. NTP processing is usually quite energy intensive. Therefore, in this section, we will concentrate on a discussion of reactor electrical energy consumption, because preliminary economic analysis indicates that the major cost of an NTP reactor system resides in the cost of the electrical power supply, assuming one uses readily-available power supplies - which are usually not well-matched to a plasma load. In some cases the power supply might be 75-90% of the plasma reactor cost. This cost is expected to fall with the development of better-matched, state-of-the-art power supplies and operation of the plasma reactor at more optimal treatment conditions.

10.6.1 Figures of Merit

A useful figure of merit for the decomposition of pollutants is defined by the energy delivered to the plasma per hazardous molecule removed from the gas stream. At any instant, this can be expressed as the following quantity obtained by solving Equation 10.13 for $\bar{E}$ and taking the derivative:

$$\gamma_i = -\frac{d\bar{E}}{d[X]} = -\frac{d[-\beta \ln(\frac{[X]}{[X]_0})]}{d[X]} = \frac{\beta}{[X]} . \tag{10.18}$$

This is the instantaneous energy cost per molecule removed; a more practically-useful parameter is the integral, or average, energy cost γ

$$\gamma = \frac{\bar{E}}{[X]_0 - [X]} = \frac{-\beta \ln(\frac{[X]}{[X]_0})}{[X]_0(1-\frac{[X]}{[X]_0})} . \tag{10.19}$$

here, the energy cost per molecule is expressed in terms of the β-value, the degree of removal, and the initial concentration.

When radical scavenging dominates radical-pollutant attack, Equation 10-18 indicates that the instantaneous energy cost per pollutant molecule removed is lower when the pollutant concentration is high. This makes intuitive sense because, at high concentration, active species always have a high probability of reacting with a target molecule. Equation 10-19 shows that the average energy cost per removed molecule is lower at lower degrees of pollutant removal and at higher initial pollutant concentration. In optimizing reactor performance, one can conceive of somehow adjusting the active species concentrations so that the ratio of pollutant concentration to active-species concentration is always relatively large. This way the probability of attack is high, while both the specific energy $\bar{E}$ and the degree of removal ($[X]/[X]_0 \sim 1$) are low.

When radical-pollutant attack dominates radical scavenging, the β-value derived from Equation 10-14 is

$$\beta = \approx [X]_0/G . \tag{10-20}$$

Inserting this into Equation 10-19 shows that, in this case, the removal energy cost is independent of the initial pollutant concentration and can be expressed as

$$\gamma = \frac{\bar{E}}{[X]_0 - [X]} = \frac{-\ln(\frac{[X]}{[X]_0})}{G\,(1-\frac{[X]}{[X]_0})} . \tag{10-21}$$

10.6.2 Example Cases

As an example, Figure 10.13 shows a plots of the degree of removal and γ (versus $\bar{E}$) for two example cases: β = 100 J/L and 1 kJ/L (for the scavenging-dominated case). The γ-value translates into an actual electrical energy cost for the process. Another convenient unit for the figure of merit is the number of kilowatt-hours required to remove a kilogram of hazardous compound (i.e., kW-hr/kg). For a γ-value of 50 eV/molecule (a model TCE mixture), approximately 10 kW-hr/kg of TCE are required. At an electrical energy cost of 5¢/kW-hr, TCE removal costs about 50¢ per kg (based only on the cost of electrical energy in the plasma - and not including the efficiency of delivering this energy to the plasma).

As an example of the case where radical attack is dominant, assume a 90% removal of the pollutant and a G-value of 10 radicals/100 eV. The average pollutant removal-energy cost is then 26 eV/molecule, independent of the initial concentration.

INSERT FIGURE 10.13 NEAR HERE

10.6.3 Optimal Removal Energy Costs

To reduce the average removal energy cost per molecule, Equation 10.19 shows that this can be achieved by reducing the β-value (improving the efficiency of radical generation and reducing the effects of scavenging) and keeping the degree of removal $[X]/[X]_0$ low.. The β-value is related to the gas mixture and the reduced electric field E/N at which the reactor operates, so these variables provide some control over the removal energy cost.

To derive the optimal γ-value, when radical scavenging is dominant, we take the limit of Equation 10-19 at very low degree of removal (i.e., $[X]/[X]_0 \sim 1$)

$$\gamma_{opt} = \lim_{\frac{[X]}{[X]_0} \to 0} \frac{-\beta \ln(\frac{[X]}{[X]_0})}{[X]_0(1-\frac{[X]}{[X]_0})} = \frac{\beta}{[X]_0} \quad . \tag{10.22}$$

This equation shows that the optimal average removal cost is obtained when the β-value is as low as possible and the initial concentration $[X]_0$ is as high as possible. For a case in which β = 100 J/L and $[X]_0$ = 500 ppm, γ_{opt} = 46 eV/molec. If the initial concentration were doubled, the removal energy cost would be halved.

In the case in which radical attack is dominant, Equations 10-20 and 10-22 gives an optimal energy removal cost of

$$\gamma_{opt} = 1/G \, . \tag{10-23}$$

For an example G-value of 10 radicals/100 eV, the optimal average removal-energy cost is approximately 10 eV/molecule.

10.7 Conclusions/Summary

Many VOCs are readily attacked by the free radicals and other active species generated in pulsed-corona- and silent-discharge-excited NTPs. In general, the degree of removal of a par-

ticular chemical species scales exponentially with the plasma energy density. The characteristic energy density that must be supplied to the active plasma volume to lower the concentration of the target pollutant to 1/e of its original value depends on the specific pollutant and the carrier gas composition. The plasma-initiated decomposition chemistry of a particular compound or mixture can be quite complicated and has been the subject of both laboratory and field investigations. NTP treatment is expected to be particularly advantageous for the simultaneous removal of multiple pollutants or for pollutants that are difficult to treat with conventional technologies. It should be emphasized that NTP is an emerging air-emissions control technology. Very few commercial systems exist. Also, for many emissions applications (chlorinated and/or fluorinated VOCs, in particular), the present forms of NTP technology are expected to be energy intensive in terms of the electrical power consumption and may require ancillary equipment (e.g., scrubbers) to handle treatment byproducts. The stand-alone application is only about a decade old; therefore, more work is needed to optimize and mature the process for widespread commercial use. Because stand-alone NTP reactors have both performance and economic limitations, some workers in this field have proposed the use of staged or hybrid systems to better match particular air-emissions control problems. Hybrid systems may be the future path for improving performance, economics, and the match to the emissions stream.

In this chapter, we have described the formation of active species in the plasma, presented a simple view of the decomposition chemistry, discussed some representative experiments with pulsed corona and silent discharge plasma reactors, have formulated a simple analytical model for pollutant decomposition and derived associated removal equations, and have defined and derived figures of merit for plasma reactor energy efficiency.

10.8 Acknowledgments

The authors would like to express their appreciation for the contributions of William McCulla, John Coogan, Michael Kang, Roger Tennant, Graydon Anderson, Paul Wantuck, Zoran Falkenstein, Hans Snyder, Harold Garcia, and Michael Garcia for their efforts in establishing and maintaining the work of the non-thermal plasma processing laboratory at Los Alamos. Thanks also go to the Strategic Environmental Research and Development Program for partially supporting this work.

10.9 References

10.1 Several very useful NTP articles appear in the following sources:

(a) B.M. Penetrante and S.E. Schultheis, Eds., *Non-Thermal Plasma Techniques for Pollution Control, NATO ASI Series, **G34**, Parts A & B;* Springer-Verlag, Berlin & Heidelberg (1993).

(b) J.-S. Chang, J.-S. and J.L. Ferreira, Eds., *Proceedings of the Second International Symposium on Non-Thermal Plasma Technology for Gaseous Pollution Control*; Catholic University of Brasilia Press, Brasilia, Brazil (1998).

(c) J.-S.Chang and B.M. Penetrante, Guest Eds., *J. Adv. Oxid. Technol.*, **2**, *Special Issue on Non-Thermal Plasma Technologies*, part of the proceedings of the Third International Conference on Advanced Oxidation Technologies, Cincinnati, OH, Oct. 26-29, 1996, (1997).

(d) *Proceeding of First International EPRI/NSF Symposium on Advanced Oxidation*, EPRI TR-102927-V2, Electric Power Research Institute, Palo Alto, CA (1993).

(e) *Abstracts, Session Overviews, and Proceedings of Second International EPRI/NSF Symposium on Environmental Applications of Advanced Oxidation Technologies*, Electric Power Research Institute, Palo Alto, CA, (1996).

(f) J.V. Heberlein, D.W. Ernie, and J.T. Roberts, Eds., *Proceedings of 12th International Symposium on Plasma Chemistry (ISPC-12)*, University of Minnesota: Minneapolis, MN, (1995).

10.2 W. von Siemens, "Uber die Elektrostatische Induktion und die Verzogerung des Stromes in Faschendrahten," *Poggendorf's Ann. Physik Chemie*, **102**, pp. 66-122 (1857).

10.3 M. Bertholot, "Sur l' Absorption de l' Azote et de l' Hydrogene Libres et Purs par les Matieres Organiques," *Acad. Sci. Compt. Rend.*, **82**, pp. 1357-1360 (1876).

10.4 G. Glockler and S.C. Lind, *The Electrochemistry of Gases and Other Dielectrics*; John Wiley and Sons, New York, (1939).

10.5 B. Eliasson and U. Kogelschatz, "Nonequilibrium Volume Plasma Chemical Processing," *IEEE Trans. Plasma Sci.*, **19**, pp. 1063-1097 (1991).

10.6 U. Kogelschatz; B. Eliasson, and W. Egli, "Dielectric-Barrier Discharges Principle and Applications," *J. de Physique IV*, 7, pp. 47-66 (1997).

10.7 J.-S. Chang, P.A. Lawless, and T. Yamamoto, "Corona Discharge Processing," *IEEE Trans. Plasma Sci.*, **19**, pp. 1152-1166 (1991).

10.8 L.A. Rosocha and R.A. Korzekwa, "Advanced Oxidation and Reduction Processes in the Gas Phase Using Non-Thermal Plasmas," *J. Adv. Oxid. Technol.* (to be published 1999).

10.9 D.E. Tevault, "Application of Plasma Technology for Proposed Military Air Purification Applications," In *Non-Thermal Plasma Techniques for Pollution Control, NATO ASI Series, Vol.* **G34**, Part A, B.M. Penetrante and S.E. Schultheis, Eds., Springer-Verlag, Berlin & Heidelberg, pp. 49-57 (1993).

10.10 L.J. Bailin, M.E. Sibert, L.A. Jonas, and A.T. Bell, "Microwave Decomposition of Toxic Vapor Simulants," *Environ. Sci. Technol.*, **9**, pp. 254-258 (1975).

10.11 S. Mukkavilli, C.K. Lee, K. Varghese, and L.L. Tavarides, "Modeling of the Electrostatic Corona Discharge Reactor," *IEEE Trans. Plasma Sci.*, **16**, pp. 652-660 (1988).

10.12 E.J. Clothiaux, J.A. Koropchack, and R.R. Moore, "Decomposition of an Organophosphorus Material in a Silent Electrical Discharge," *Plasma Chem. Plasma Process.*, **4**, pp. 15-20 (1984).

10.13 M.E. Fraser, D.A. Fee, and R.S. Sheinson, "Decomposition of Methane in an AC Discharge," *Plasma Chem. Plasma Process.*, **5**, pp. 163-173 (1985).

10.14 D.E. Tevault, "Plasma Reactions of Methane in Nitrogen and Nitrogen/Oxygen Carriers by Matrix Isolation FTIR Spectroscopy," *Plasma Chem. Plasma Process.*, **5**, pp. 369 (1985).

10.15 M.E. Fraser, H.G. Eaton, and R.S. Sheinson, "Initial Decomposition Mechanisms of Dimethyl Methyphosphonate in an Alternating Current Discharge," *Environ. Sci. Technol.*, **19**, pp. 946-949 (1985).

10.16 W.C. Neely, "The Decomposition of Gas Phase Formaldehyde by Plasma Discharge," *Proceedings of the 1984 Scientific Conference on Chemical Defense Research*, US Army CRDEC-SP-85006, (1985).

10.17 M.E. Fraser and R.S. Sheinson, "Electric Discharge-Induced Oxidation of Hydrogen Cyanide," *Plasma Chem. Plasma Process.*, **6**, pp. 27-38 (1986).

10.18 N.W. Frank and S. Hirano, "The History of Electron Beam Processing for Environmental Pollution Control and Work Performed in the United States," in *Non-Thermal Plasma Techniques for Pollution Control, NATO ASI Series,* **G34**, *Part B,* B.M. Penetrante and S.E. Schultheis, Eds., Springer-Verlag: Berlin & Heidelberg, pp. 1-26 (1993).

10.19 R.C. Slater and D.H. Douglas-Hamilton, "Electron-Beam-Initiated Destruction of Low Concentrations of Vinyl Chloride in Carrier Gases," *J. Appl. Phys.*, **52**, pp. 5820-5828 (1981).

10.20 H.-R. Paur, "Removal of Volatile Organic Compounds from Industrial Off-Gas," in *Non-Thermal Plasma Techniques for Pollution Control, NATO ASI Series,* **G34**, *Part B,* B.M. Penetrante and S.E. Schultheis, Eds., Springer-Verlag: Berlin & Heidelberg, pp.77-89 (1993).

10.21 A.G. Chmielewski, E. Iller, Z. Zimek, M. Romanowski, and K. Koperski, "Pilot-Plant for Flue-Gas Treatment: Continuous Operation Tests," *Radiat. Phys. Chem.*, **46**, pp. 1063-1066 (1995).

10.22 S. Masuda, "Pulsed Corona-Induced Plasma Chemical Process: a Horizon of New Plasma Chemical Technologies," Pure Appl. Chem. **60**, pp. 727-731 (1988).

10.23 S. Masuda and H. Nakao, "Control of NO_x by Positive and Negative Pulsed Corona Discharges," *IEEE Trans. Ind. Appl.*, **26**, pp. 374-382 (1990).

10.24 A. Mizuno, J.S. Clements, and R.H. Davis, "A Method for the Removal of Sulfur-Dioxide from Exhaust Gas Utilizing Pulsed Streamer Corona for Electron Energization," *IEEE Trans. Ind. Appl.*, **IA-22**, pp. 516-521 (1986).

10.25 I. Gallimberti, "Impulse Corona Simulation for Flue Gas Treatment," *Pure Appl. Chem.*, **60**, pp. 663-674 (1988).

10.26 G. Dinelli, L. Civitano, and M. Rea, "Industrial Experiments on Pulse Corona Simultaneous Removal of NO_x and SO_x from Flue Gas," *IEEE Trans. Ind. Appl.* **26N**, pp. 535-541 (1990).

10.27 L. Civitano, "Industrial Applications of Pulsed Corona Processing to Flue Gas," in *Non-Thermal Plasma Techniques for Pollution Control, NATO ASI Series, Vol.* **G34**, *Part B*, B.M. Penetrante and S.E. Schultheis, Eds., Springer-Verlag, Berlin & Heidelberg, pp. 103-130 (1993).

10.28 P.A. Vitello, B.M. Penetrante, and J.N. Bardsley, "Multi-Dimensional Modeling of the Dynamic Morphology of Streamer Coronas," in *Non-Thermal Plasma Techniques for Pollution Control, NATO ASI Series* **G34**, Part A, B.M. Penetrante and S.E. Schultheis, Eds., Springer-Verlag: Berlin & Heidelberg, pp. 249-271 (1993).

10.29 M.C. Wang, and E.E. Kunhardt, "Streamer Dynamics," *Phys. Rev. A*, **42**, pp. 2366-2373 (1990).

10.30 G.V. Nadis, "*Modeling of Plasma Chemical Processes in Pulsed Corona Discharges,*" *J. Phys. D-Appl. Phys.*, **30**, pp. 1214-1218 (1997).

10.31 D. Evans, L.A. Rosocha, G.K. Anderson, J.J. Coogan, and M.J. Kushner, "Plasma Remediation of Trichloroethylene in Silent Discharge Plasmas," *J. Appl. Phys.*, **74**, pp. 5378-5386 (1993).

10.32 J.J. Lowke and R. Morrow, "Theoretical Analysis of Removal of Oxides of Sulfur and Nitrogen in Pulsed Operation of Electrostatic Precipitators," *IEEE Trans. Plasma Sci.*, **23**, pp. 661-671 (1995).

10.33 J. Li, W. Sun, B. Pashaie, and S.K. Dhali, "Streamer Discharge Simulation in Flue Gas," *IEEE Trans. Plasma Sci.*, **23**, pp. 672-678 (1995).

10.34 M.G. Grothaus, R.K. Hutcherson, R.A. Korzekwa, and R. Roush, "Coaxial Pulsed Corona Reactor for Treatment of Hazardous Gases," *Proceedings of 9th IEEE International Pulsed Power Conference*, pp. 180-183 (1993).

10.35 B.M. Penetrante, M.C. Hsiao, J.N. Bardsley, B.T. Merritt, G.E. Voghtlin, P.H. Wallman, A. Kuthi, C.P. Burkhart, and J.R. Bayless "Electron-Beam and Pulsed Corona Processing of Carbon-Tetrachloride in Atmospheric-Pressure Gas Streams," *Phys. Lett. A*, **209**, pp. 69-77 (1995).

10.36 B.M. Penetrante, M.C. Hsiao, J.N. Bardsley, B.T. Merritt, G.E. Voghtlin, P.H. Wallman, A. Kuthi, C.P. Burkhart, and J.R. Bayless "Decomposition of Methylene-Chloride by Electron-Beam and Pulsed Corona Processing," *Phys. Lett. A*, **235**, pp. 76-82 (1997).

10.37 B.M. Penetrante, M.C. Hsiao, J.N. Bardsley, B.T. Merritt, G.E. Voghtlin, P.H. Wallman, A. Kuthi, C.P. Burkhart, and J.R. Bayless "Electron-Beam and Pulsed Corona Processing

of Volatile Organic-Compounds in Gas Streams," *Pure Appl. Chem.*, **68**, pp. 1083-1087 (1996).

10.38 M.C. Hsiao, B.T. Merritt, B.M. Penetrants, G.E. Voghtlin, and P.H. Wallman, "Plasma-Assisted Decomposition of Methanol and Trichloroetylene in Atmospheric-Pressure Air Streams by Electrical-Discharge Processing," *J. Appl. Phys.*, **78**, pp. 3451-3456 (1995).

10.39 R.A. Korzekwa, L.A. Rosocha, and Z. Flakenstein, "Experimental Results Comparing Pulsed Corona and Dielectric Barrier Discharges for Pollution Control," *Proceedings of 11th IEEE International Pulsed Power Conference*, G. Cooperstein and I. Vitkovitsky, Eds., Omnipress, Madison, WI, CD ROM: 97CH36127, pp. 97-102 (1998).

10.40 V. Puchkarev and M. Gundersen, "Energy Efficient Plasma Processing of Gaseous Emission Using a Short Pulse Discharge," *Appl. Phys. Lett.*, **71**, pp. 3364-3366 (1997).

10.41 E. H.W.M. Smulders, B.E.J.M. van Heesch, and S.S.V.B. van Paasen, "Pulsed Power Corona Discharges for Air Pollution Control," *IEEE Trans. Plasma Sci.*, **26**, pp. 1476-1484 (1998).

10.42 W.C. Neely, E.I. Newhouse, E.J. Clothiaux, and C.A. Gross, "Decomposition of Complex Molecules Using Silent Discharge Plasma Processing," in *Non-Thermal Plasma Techniques for Pollution Control, NATO ASI Series,* **G34**, *Part B*, B.M. Penetrante and S.E. Schultheis, Eds., Springer-Verlag, Berlin & Heidelberg, pp. 309-320 (1993).

10.43 D.G. Storch and M.J. Kushner, "Destruction Mechanisms for Formaldehyde in Atmospheric-Pressure Low-Temperature Plasmas," *J. Appl. Phys.*, **73**, pp. 51-55 (1993).

10.44 L.A. Rosocha, G.K. Anderson, L.A. Bechtold, J.J. Coogan, H.G. Heck, M. Kang, W.H. McCulla, R.A. Tennant, and P.J. Wantuck, In *Non-Thermal Plasma Techniques for Pollution Control, NATO ASI Series,* **G34**, *Part B*, B.M. Penetrante and S.E. Schultheis, Eds., Springer-Verlag, Berlin & Heidelberg, pp. 281-308 (1993).

10.45 L.A. Rosocha, "Processing of Hazardous Chemicals Using Silent-Electrical-Discharge Plasmas," Chapter 11 in *Environmental Aspects in Plasma Science*; W. Manheimer, L.E. Sugiyama, and T.H. Stix, Eds., American Institute of Physics Press: Woodbury, NY, pp. 261-298 (1997).

10.46 J.J. Coogan, L.A. Rosocha, M.J. Brower, M. Kang, and C.A. Schmidt, "Scaling of Silent Electrical Discharge Reactors for Hazardous Organics Destruction," *Proceedings of 11th Ozone World Congress, Ozone in Water and Wastewater Treatment, Vol. 2*, Section S-15, pp. 25-28 (1993).

10.47 Z. Falkenstein, "Processing of C_3H_7OH, C_2HCl_3 and CCl_4 in Flue Gases Using Silent Discharge Plasmas (SDPs), Enhanced by (V)UV at 172 nm and 253.7 nm," *J. Adv. Oxid. Technol.*, **2**, pp. 223-238 (1997).

10.48 L.N. Krasnoperov, L.G. Krishtopa, J.W. Bozzelli, "Study of Volatile Organic Compounds Destruction by Dielectric Barrier Corona Discharge," *J. Adv. Oxid. Technol.*, **2**, pp. 248-256 (1997).

10.49 H.R. Snyder and G.K. Anderson, "Effect of Air and Oxygen Content on the Dielectric Barrier Discharge Decomposition of Chlorobenzene," *IEEE Trans. Plasma Sci.*, **26**, pp. 1695-1609 (1999).

10.50 J.W. Virden, W.O. Heath, S.C. Goheen, M.C. Miller, G.M. Mong, and R.L. Richardson, *Proceedings of Spectrum '92 conference, Boise, ID, Pacific Northwest Laboratory Document PNL-SA-20741*, (1992).

10.51 C.M. Nuñez, D.H. Ramsey, W.H. Ponder, J.H. Abbott, L.E. Hamel, and P.H. Kariher, "Corona Destruction: An Innovative Control Technology for VOCs and Air Toxics," *J. Air & Waste Management Assoc.*, **43**, pp. 242-247 (1993).

10.52 L. Bromberg, D.R. Cohn, M. Koch, R.M. Patrick, and P. Thomas, "Decomposition of Dilute Concentrations of Carbon Tetrachloride in Air by an Electron-Beam Generated Plasma," *Phys. Lett. A*, **173**, pp. 293-299 (1993).

10.53 M. Koch, D.R. Cohn, R.M. Patrick, M.P. Scheutze, L. Bromberg, D. Reilly, and P. Thomas, " *Phys. Lett A*, **184**, pp. 109-113 (1993).

10.54 S.M. Matthews, A.J. Boegel, and J.A. Loftis, "Radiolytic Decomposition of Environmental Contaminants and Site Remediation Using an Electron Accelerator," *Remediation*, **Autumn**, pp. 459-481 (1993).

10.55 S.A. Vitale, K. Hadidi, D.R. Cohn, and P. Falkos, "Electron-Beam Generated Plasma Decomposition of 1,1,1-Trichloroethane," *Plasma Chem. Plasma Process.*, **16**, pp. 651-668 (1996).

10.56 D.R. Cohn, "Hot and Cold Plasma Processing of Waste," Chapter 9 in *Environmental Aspects in Plasma Science*; W. Manheimer, L.E. Sugiyama, and T.H. Stix, Eds., American Institute of Physics Press, Woodbury, NY, pp. 209-229 (1997).

10.57 A. Mizuno and H. Ito, "Basic Performance of an Electrically Augmented Filter Consisting of Packed Ferroelectric Pellet Layer," *J. Electrostatics*, **25**, pp. 97-107 (1990).

10.58 T. Yamamoto, P.A. Lawless, M.K. Owen, and D.S. Ensor, "Decomposition of Volatile Organic Compounds by a Packed-Bed Reactor and a Pulsed-Corona Plasma Reactor," in *Non-Thermal Plasma Techniques for Pollution Control, NATO ASI Series,* **G34**, *Part B*, B.M. Penetrante and S.E. Schultheis, Eds., Springer-Verlag: Berlin & Heidelberg, pp. 223-237 (1993).

10.59 B. Lermer, J. Birmingham, R. Tonkyn, S. Barlow, and T. Orlando, "Decomposition of Trichloroethylene by a Large Scale, High Flow Packed-Bed Gas Phase Corona Reactor," *Proceedings of 12th International Symposium on Plasma Chemistry (ISPC-12)*, J.V. Heberlein, D.W. Ernie, and J.T. Roberts, Eds., University of Minnesota: Minneapolis, MN, pp. 697-703 (1996).

10.60 R.G. Tonkyn, S.E. Barlow, and T.M. Orlando, "Destruction of Carbon-Tetrachloride in a Dielectric Barrier/Packed-Bed Corona Reactor," *J. Appl. Phys.*, **80**, pp. 4877-4886 (1996).

10.61 S. Masuda, "Destruction of Gaseous Pollutants and Air Toxics by Surface Discharge Induced Plasma Chemical Process (SPCP) and Pulse Corona Induced Chemical Process (PPCP)," in *Non-Thermal Plasma Techniques for Pollution Control, NATO ASI Series,*

G34, *Part B*, B.M. Penetrante and S.E. Schultheis, Eds., Springer-Verlag: Berlin & Heidelberg, pp. 199-209 (1993).

10.62 V.F. Puchkarev, G.J. Roth, and M.A. Gunderson, "Toxic Gas Decomposition by Surface Discharge," *IEEE Conference Record - Abstracts, 1994 International Conference on Plasma Science*, Santa Fe, NM, Paper IE6, pp. 88-89 (1994).

10.63 H. Raether, *Electron Avalanches and Breakdown in Gases*, Butterworths, London (1964).

10.64 Yu. P. Raizer, *Gas Discharge Physics*, Springer-Verlag, New York (1991).

10.65 Yu. D. Korolev and G.A. Mesyats, *Physics of Pulsed Breakdown in Gases*, URO-Press, Yekaterinburg, Russa, (1998).

10.66 M. Rea and K. Yan, "Evaluation of Pulse Voltage Generators," *IEEE Trans. Plasma Sci.*, **31**, pp. 507-512 (1995).

10.67 Y.L.M. Creyghton, E.M. van Veldhuizen, and W.R. Rutgers "Electrical and Optical Study of Pulsed Positive Corona," in *Non-Thermal Plasma Techniques for Pollution Control, NATO ASI Series,* **G34**, *Part A*, B.M. Penetrante and S.E. Schultheis, Eds., Springer-Verlag: Berlin & Heidelberg, pp. 205-230 (1993).

10.68 W.L. Morgan, M. Jacob, and E.R. Fisher, In *Proceedings of 12th International Symposium on Plasma Chemistry (ISPC-12)*, J.V. Heberlein, D.W. Ernie, and J.T. Roberts, Eds., University of Minnesota, Minneapolis, MN, pp. (1995).

10.69 S.A. Vitale, K. Hadidi, D.R. Cohn, and P. Falkos, "The Effect of a Carbon-Carbon Double-Bond on Electron Beam-Generated Plasma Decomposition of Trichloroethylene and 1,1,1-Trichloroethane," *Plasma Chem. Plasma Proc.*, **17**, pp. 59-78 (1997).

10.70 B.M. Penetrante, M.C. Hsiao, J.N. Bardsley, B.T. Merritt, G.E. Vogtlin, and P.H. Wallman, "," *Proceedings of the Second International Symposium on Environmental Applications of Advanced Oxidation Technologies*, Electric Power Research Institute, *Section 5*, pp. 74-88 (1997).

10.71 D.G. Storch, M.B. Chang, M.J. Rood, and M.J. Kushner, "Modeling and Diagnostics of Dielectric Barrier Discharge Destruction of CCl_4, *"Unpublished progress report to Los Alamos National Laboratory* (1991).

10.72 S. Futamura, A.H. Zhang, and T. Yamamoto, "The Dependence of Nonthermal Plasma Behavior of VOCs on Their Chemical Structures," *J. Electrostatics*, **42**, pp. 51-62 (1997).

10.73 B.M. Penetrante, J.N. Bardsley, and M.C. Hsiao, "Kinetic-Analysis of Nonthermal Plasmas Used for Pollution-Control, *Japanese J. Appl. Phys., Part 1-Regular papers Short Notes & Review Papers*, **36**, pp. 5007-5017 (1997).

10.74 B.M. Penetrante, M.C. Hsiao, J.N. Bardsley, B.T. Merritt, G.E. Voghtlin, A. Kuthi, C.P. Burkhart, and J.R. Bayless, "Identification of Mechanisms for Decomposition of Air-Pollutants by Nonthermal Plasma Processing," *Plasma Sources Sci. Tecnol.*, **6**, pp. 251-259 (1997).

10.75 J.D. Skalny, V. Sobek, P. Lukac, "Negative Corona Induced Decomposition of CCl_2F_2," in *Non-Thermal Plasma Techniques for Pollution Control, NATO ASI Series, **G34**, Part A*,

B.M. Penetrante and S.E. Schultheis, Eds., Springer-Verlag, Berlin & Heidelberg, pp. 151-165 (1993).

10.76 J.J. Coogan, and A.S. Jassal, "Silent Discharge Plasma (SDP) for Point-of-Use (POU) Abatement of Volatile Organic Compound (VOC) Emissions: Final Report (ESHC003)," *SEMATECH Technology Transfer Document 97023244A-ENG* (1997).

10.77 T.C. Manley, "The Electrical Characteristics of the Ozonator Discharge," *Trans. Electrochem. Soc.*, **84**, pp. 83-96 (1943).

10.78 F. Westley, J.T. Herron, R.F. Hampson, and W.G. Mallard, Eds., *NIST Reference Database* **17**, National Institute of Standards and Technology, Gaithersburg, MD, (1994).

10.79 P. Ott, D. Helf, and K. Kirchner, "Oxidation of Trichloroethylene with OH-Radicals and O-Atoms," *Dechema-Monographs, VCH Verlagsgesellschaft*, **104**, pp. 91-98 (1987).

10.80 L.L. Alston, *High-Voltage Technology*, Oxford University Press, London, (1986).

10.81 J.R. Bolton, K.G. Bircher, W. Tumas, and C.A. Tolman, "Figures-of-Merit for the Technical Development and Application of Advanced Oxidation processes," *J. Adv. Oxid. Technol.*, **1**, pp. 13-17 (1996).

10.82 D.L. Baulch, J. Duxbury, S.J. Grant, and D.C. Montague, "Evaluated Kinetic Data for High Temperature Reactions, Vol. 4, Homogeneous Gas Phase Reactions of Halogen- and Cyanide-Containing Species, *J. Phys. Chem. Ref. Data*, **10**, Suppl. 1, 1-1 (1981).

10.83 D.L. Baulch, R.A. Cox, P.J. Crutzen, R.F. Hampson, Jr., J.A. Kerr, J. Troe, and R.T. Watson, "Evaluated Kinetic and Photochemical Data for Atmospheric Chemistry: Supplement I CODATA Task Group on Chemical Kinetics," *J. Phys. Chem. Ref. Data*, **11**, pp. 327-400 (1982).

Figure Captions

Figure 10.1: Schematic diagrams of pulsed corona and dielectric barrier non-thermal plasma reactors.

Figure 10.2: Plot of typical specific energies versus gas residence time for pulsed corona and silent electrical discharge reactors.

Figure 10.3: Representative non-thermal plasma (negative corona and dielectric barrier reactors) decomposition plots taken from the literature. (a) Chlorobenzene (C_6H_5Cl) in synthetic air, after Krasnoperov et al [10.48]; (b) CFC-12 (CCl_2F_2) in dry air, after Skalny et al [10.75]; (c) TCE in dry air, after present authors and Falkenstein [10.47]; (d) Methanol (CH_3OH), after Hsiao et al [10.38].

Figure 10.4: Electrical schematic diagram of pulsed corona apparatus used in Los Alamos experiments.

Figure 10.5: Voltage and current waveforms for pulsed corona reactor when operating with ambient-pressure (~ 580 torr), room-temperature, dry air.

Figure 10.6: Electrical schematic diagram of ac-driven dielectric-barrier (silent discharge) reactor apparatus used in described experiments.

Figure 10.7: Typical electrical waveforms for silent discharge reactor: (a) Voltage (V) and transferred-charge (Q); (b) Charge-voltage (Q,V) plot (parallelogram representing deposited plasma energy per cycle).

Figure 10.8: Schematic diagram of analytical-chemistry diagnostics setup for pulsed corona and silent discharge experiments.

Figure 10.9: Measured removal plots for TCE (200 ppm in dry air), comparing pulsed corona and silent discharge reactors.

Figure 10.10: Measured removal plots for MEK (1,000 ppm in dry air), comparing pulsed corona and silent discharge reactors.

Figure 10.11: Example plots derived from the simple radical-initiated-decomposition model, for different initial pollutant concentrations. (a) case for which rate of radical attack dominates rate of radical scavenging; (b) case for which radical scavenging dominates radical attack. Note that for the second case, the decomposition plot is only weakly dependent on initial pollutant concentration and that the dependence increases at higher degrees of removal.

Figure 10.12: Example plot for the removal of methyl chloride (CH_3Cl) by OH radicals, derived from the simple radical-initiated-decomposition model when radical-radical scavenging is dominant.

Figure 10.13: Plots of the degree of removal and removal-energy cost per molecule for two example β-values, in the case in which radical scavenging is dominant.

Figure 10.1

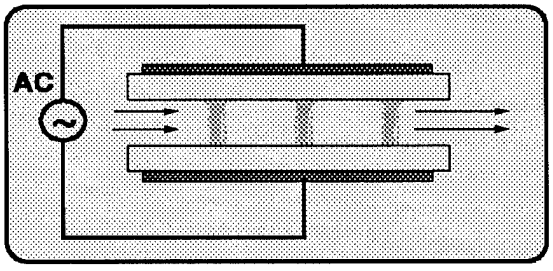

Silent discharge
(dielectric-barrier discharge)

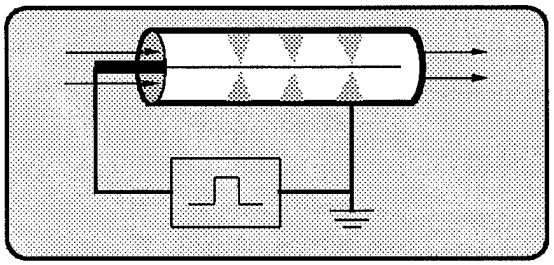

Pulsed or DC corona

Figure 10.2

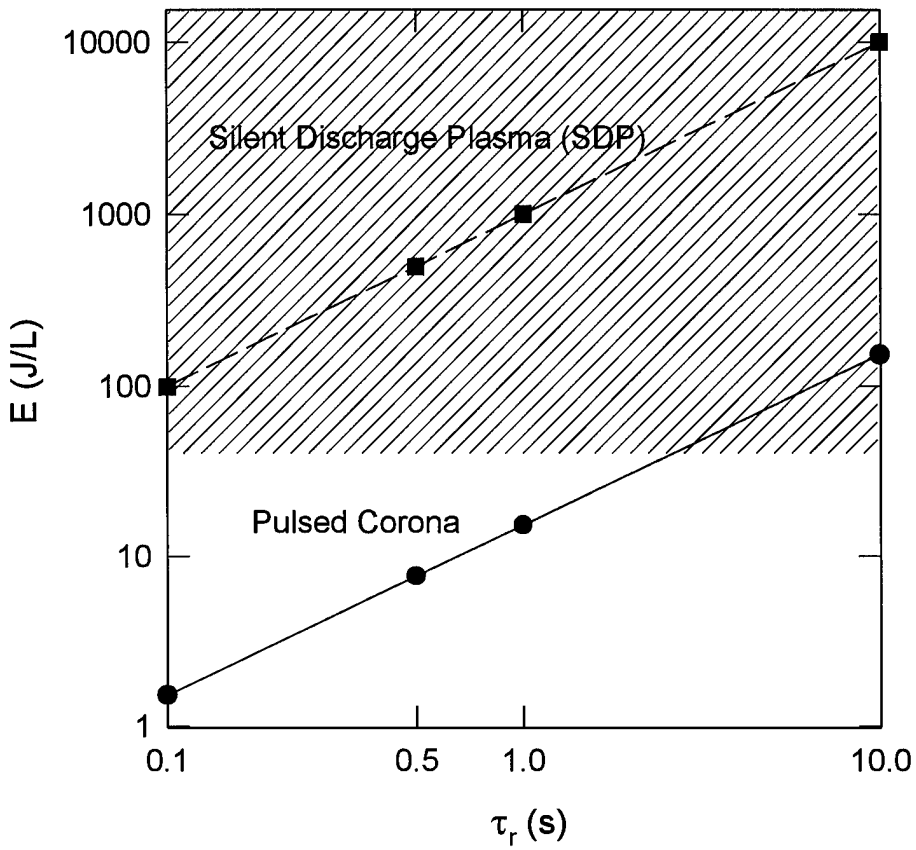
10000
1000
100
10
1
E (J/L)
Silent Discharge Plasma (SDP)
Pulsed Corona
0.1
0.5
1.0
10.0
τr (s)

Figures 10.3a & 10.3b

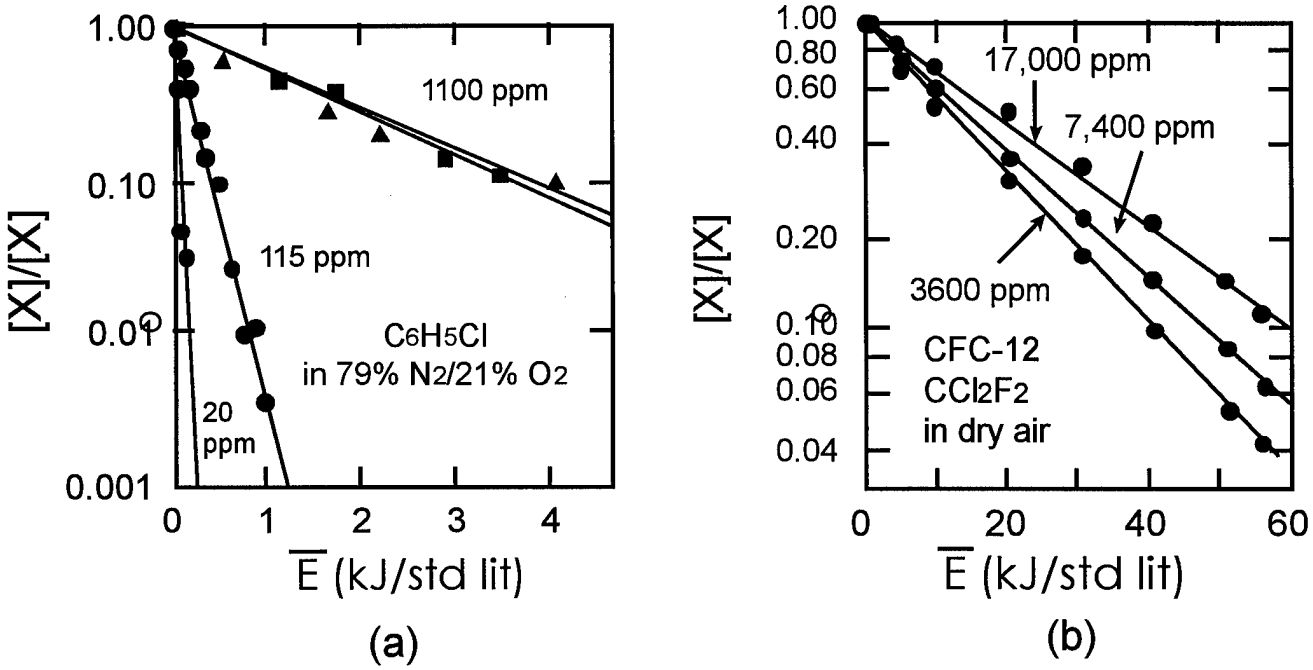

Figure 10.3c

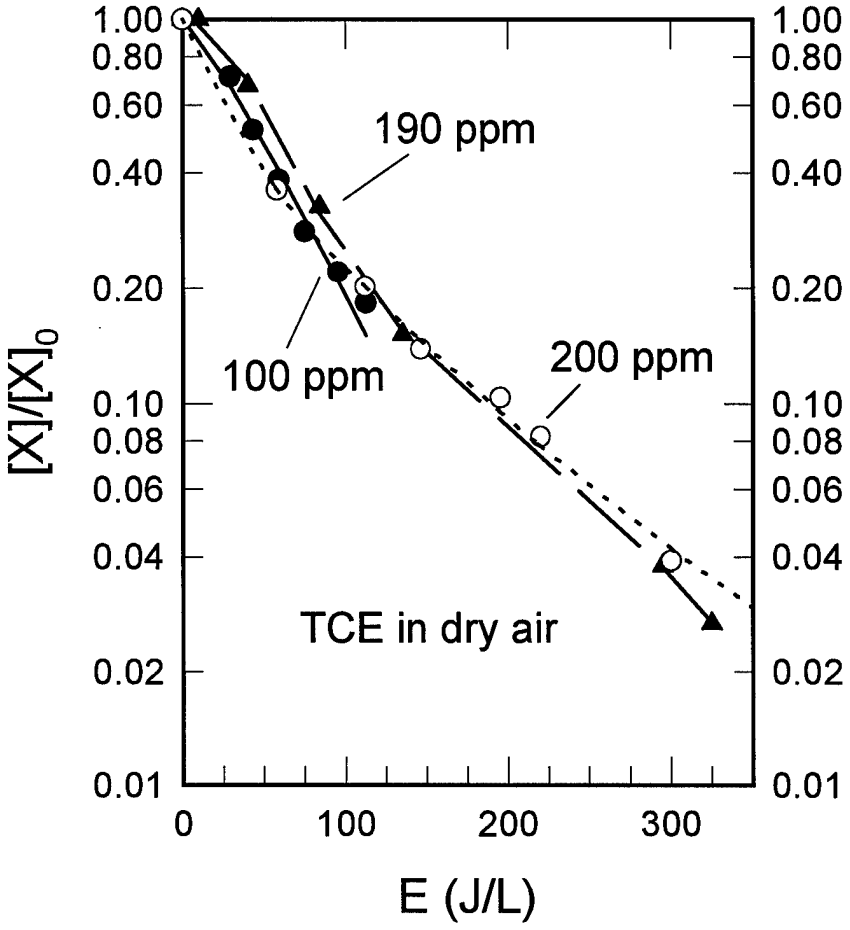
1.00
0.80
0.60
0.40
0.20
0.10
0.08
0.06
0.04
0.02
0.01
[X]/[X]0
190 ppm
100 ppm
200 ppm
TCE in dry air
0
100
200
300
E (J/L)

Figure 10.3d

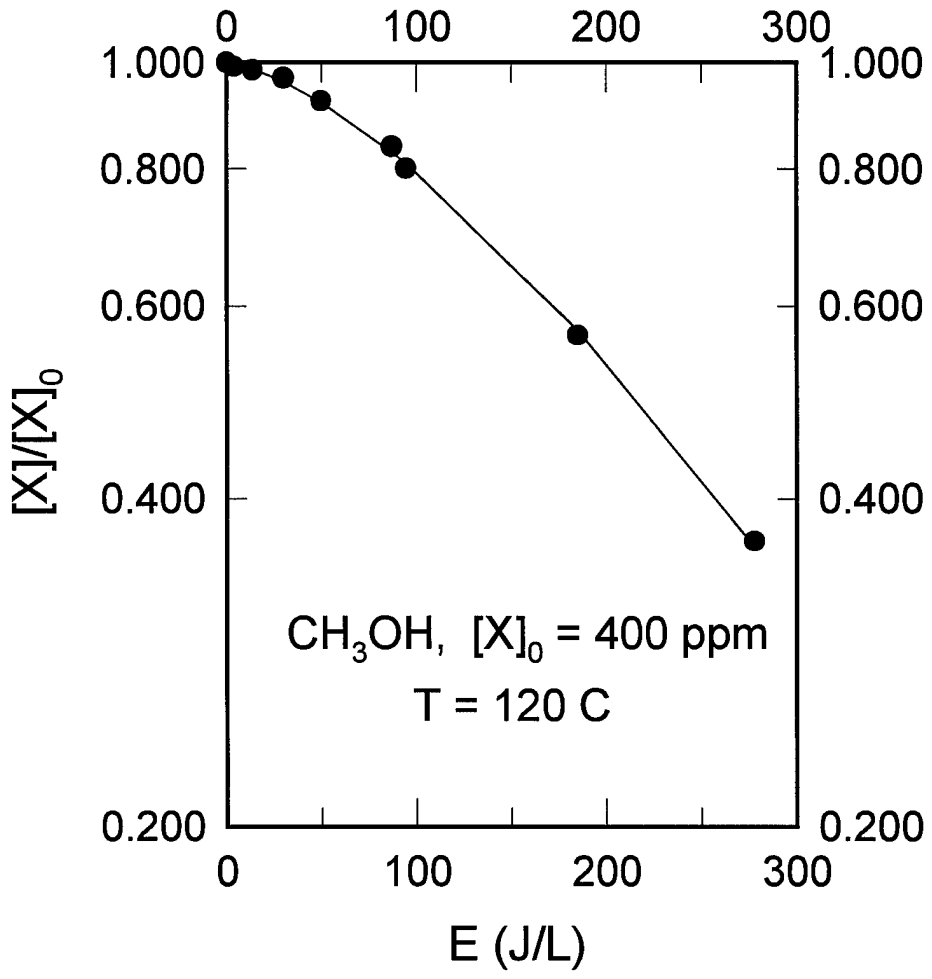
0
100
200
300
1.000
0.800
0.600
0.400
0.200
[X]/[X]0
CH3OH, [X]0 = 400 ppm
T = 120 C
E (J/L)

Figure 10.4

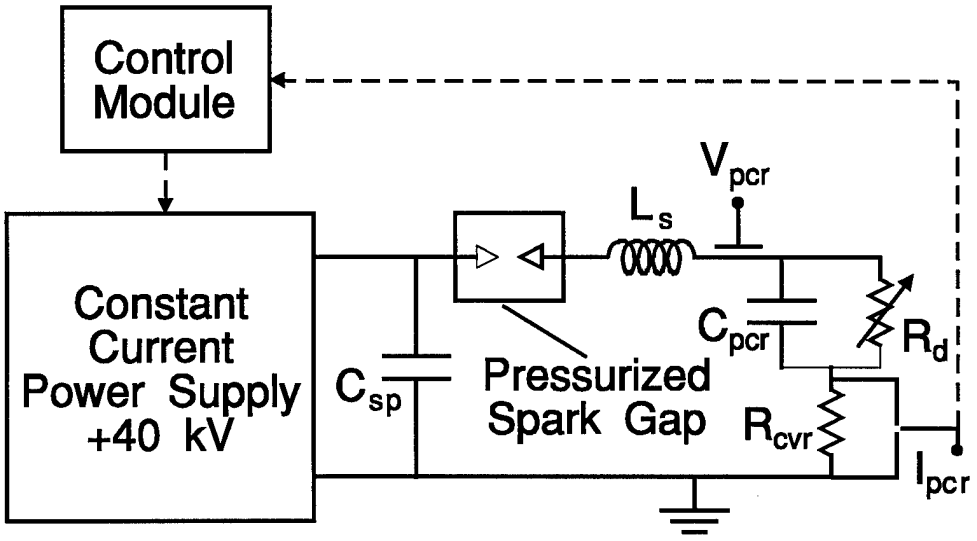
Control Module
Constant Current Power Supply +40 kV
V_{pcr}
L_s
C_{pcr}
R_d
C_{sp}
Pressurized Spark Gap
R_{cvr}
I_{pcr}

Figure 10.5

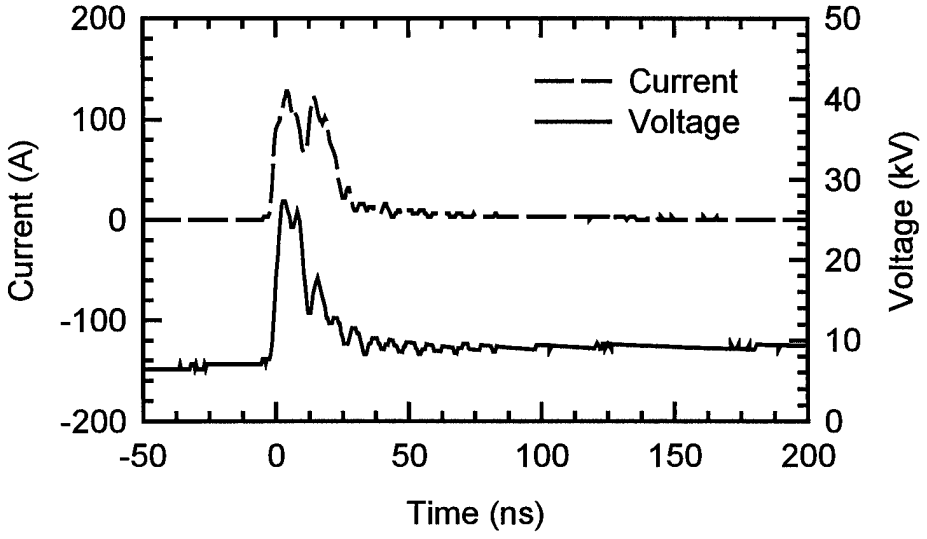
200
100
0
-100
-200
Current (A)
-50
0
50
100
150
200
Time (ns)
50
40
30
20
10
0
Voltage (kV)
Current
Voltage

Figure 10.6

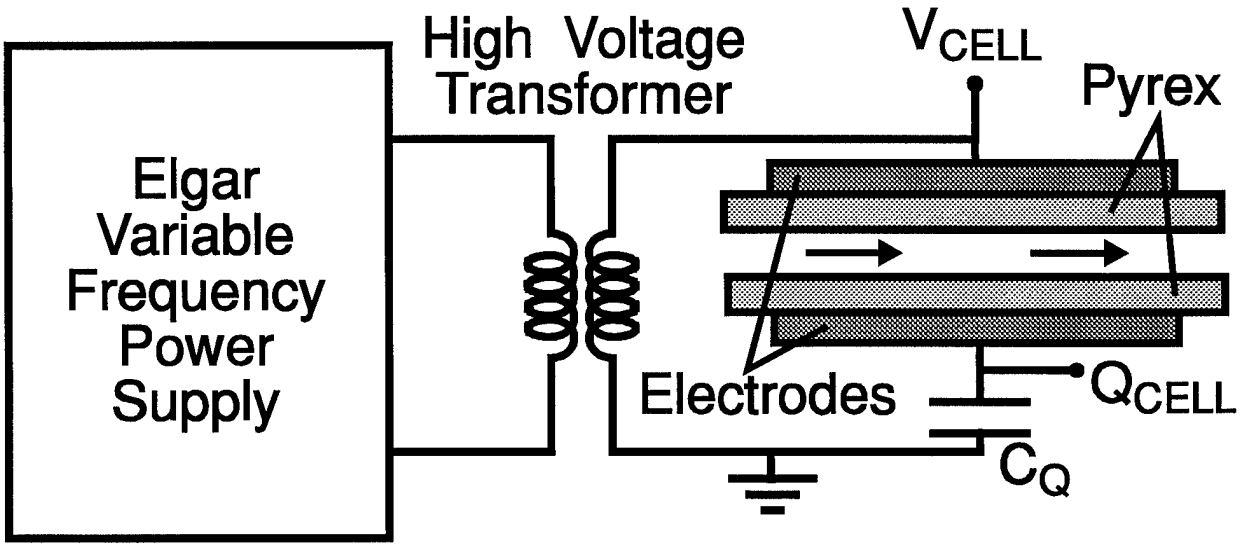
Elgar
Variable
Frequency
Power
Supply
High Voltage
Transformer
V_{CELL}
Pyrex
Electrodes
Q_{CELL}
C_Q

Figures 10.7a (upper) & 10.7b (lower)

a)

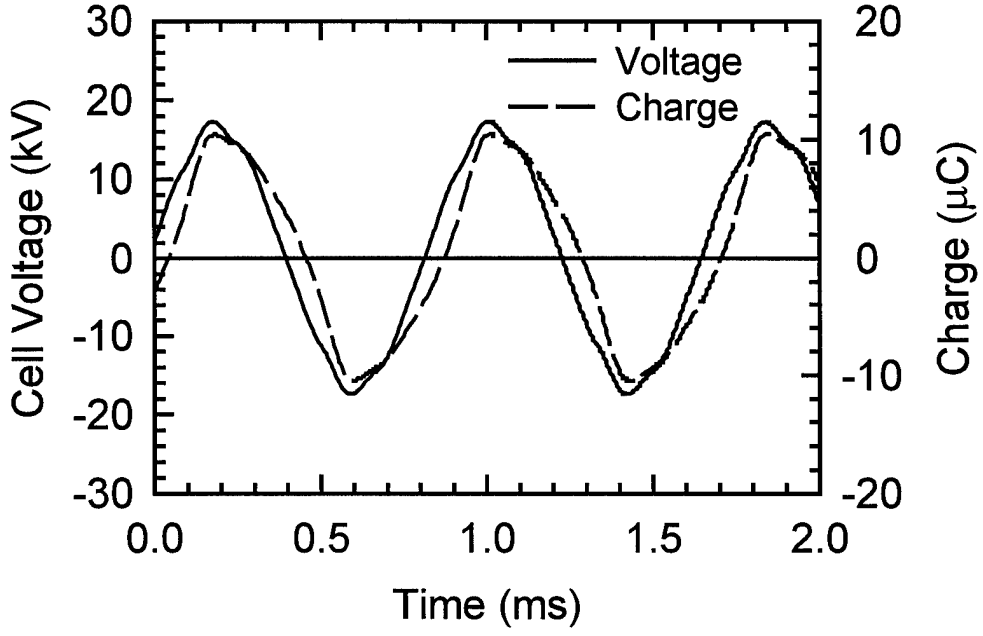

b)

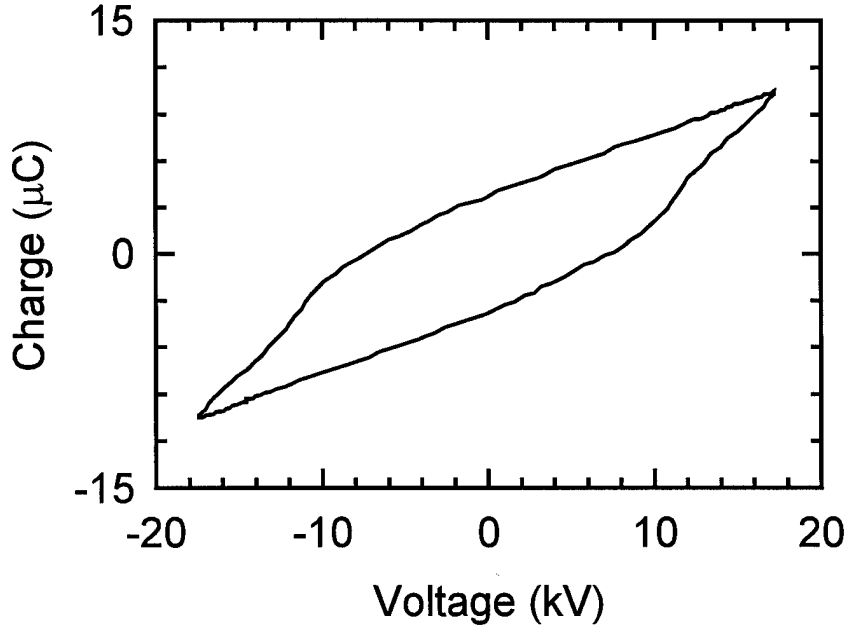

Figure 10.8

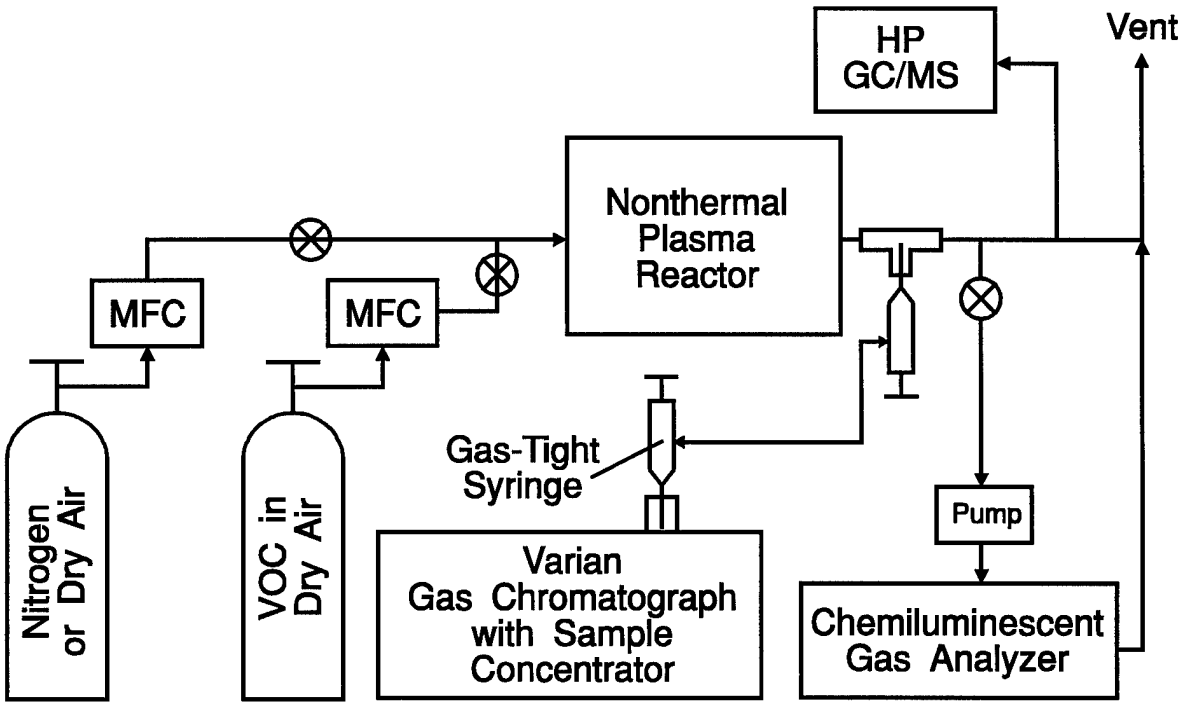
HP
GC/MS
Vent
Nonthermal
Plasma
Reactor
MFC
MFC
Nitrogen
or Dry Air
VOC in
Dry Air
Gas-Tight
Syringe
Pump
Varian
Gas Chromatograph
with Sample
Concentrator
Chemiluminescent
Gas Analyzer

Figure 10.9

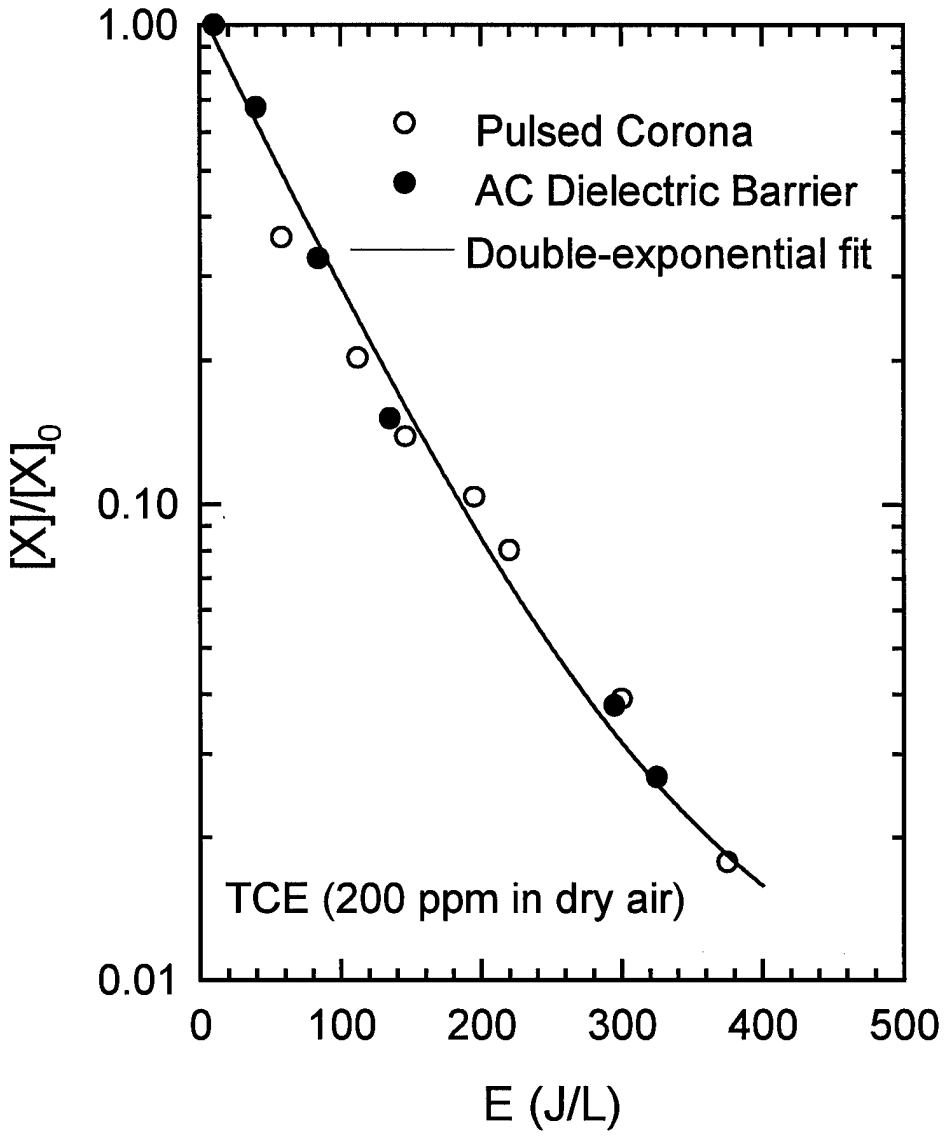
1.00
0.10
0.01
[X]/[X]0
Pulsed Corona
AC Dielectric Barrier
Double-exponential fit
TCE (200 ppm in dry air)
0
100
200
300
400
500
E (J/L)

Figure 10.10

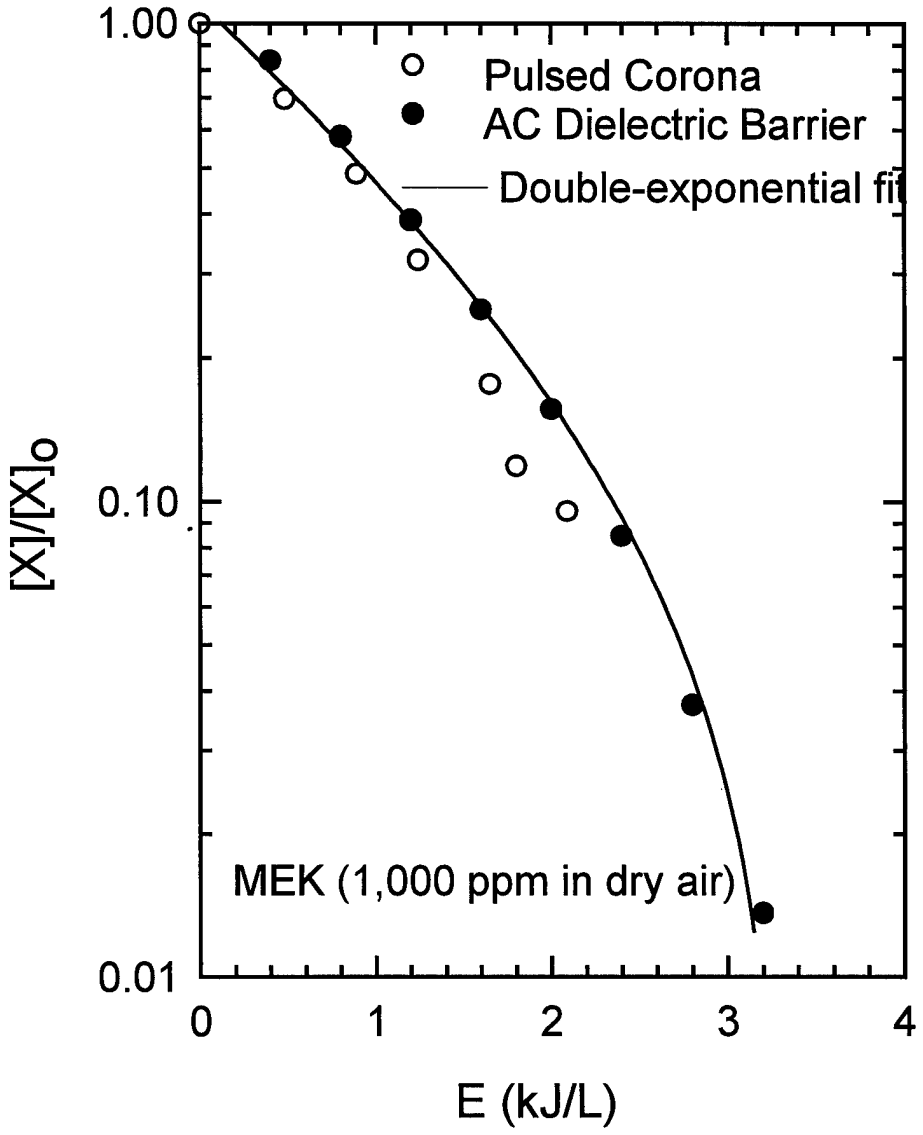
1.00
0.10
0.01
[X]/[X]o
Pulsed Corona
AC Dielectric Barrier
Double-exponential fi
MEK (1,000 ppm in dry air)
0
1
2
3
4
E (kJ/L)

Figure 10.11a

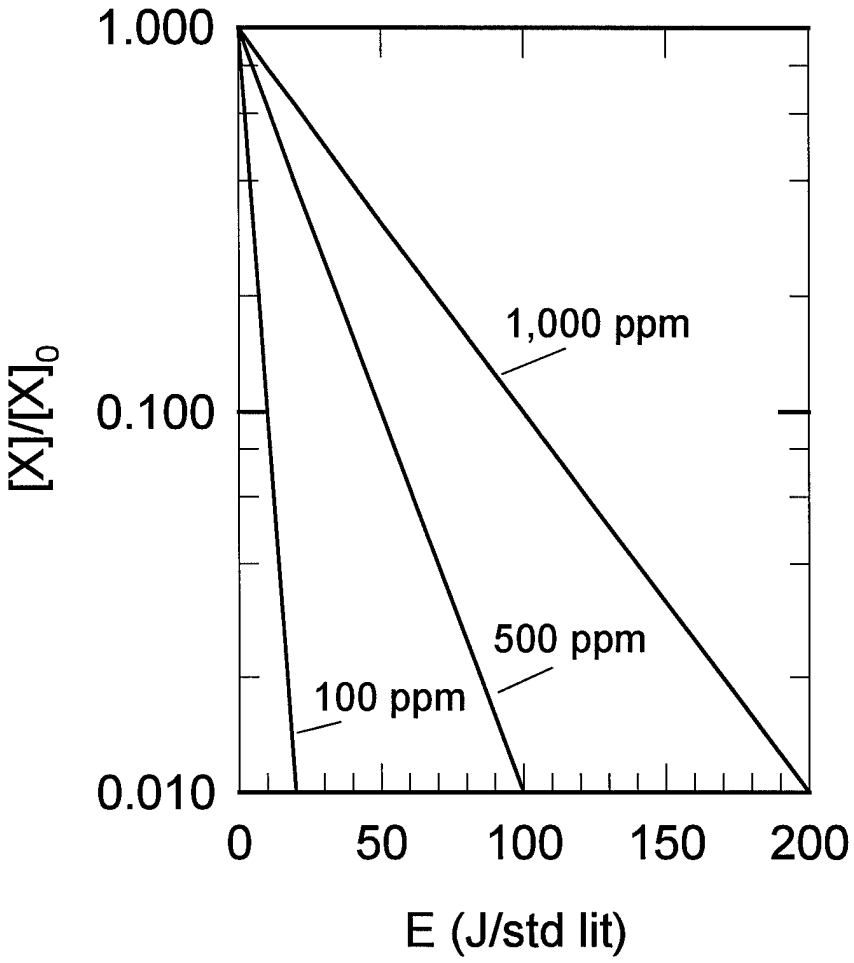

Figure 10.11b

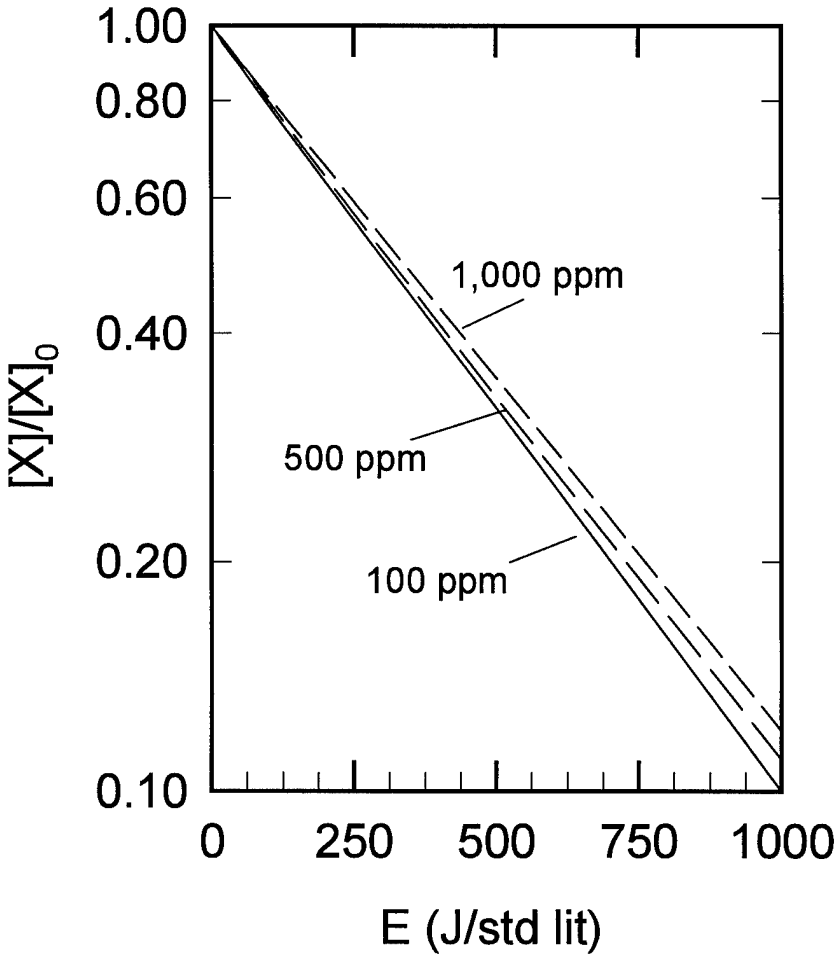

Figure 10.12

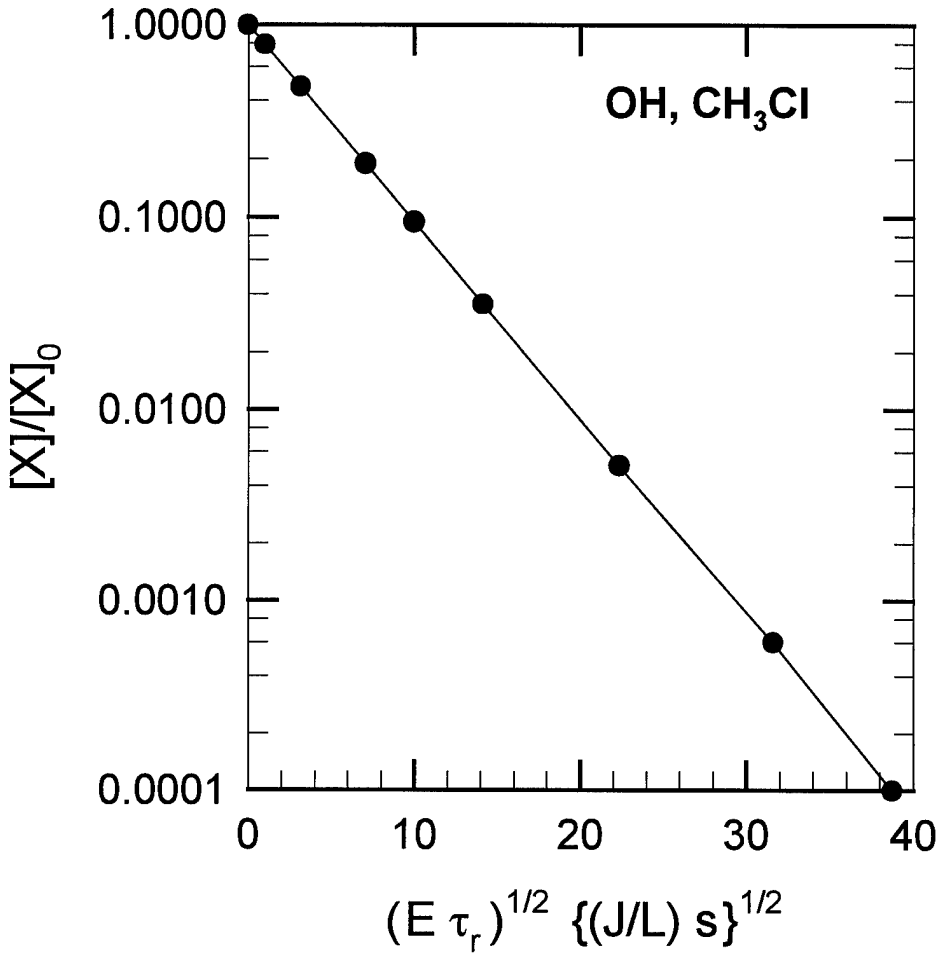
1.0000
0.1000
0.0100
0.0010
0.0001
[X]/[X]$_0$
OH, CH_3Cl
0
10
20
30
40
$(E\ \tau_r)^{1/2}$ {(J/L) s}$^{1/2}$

Figure 10.13

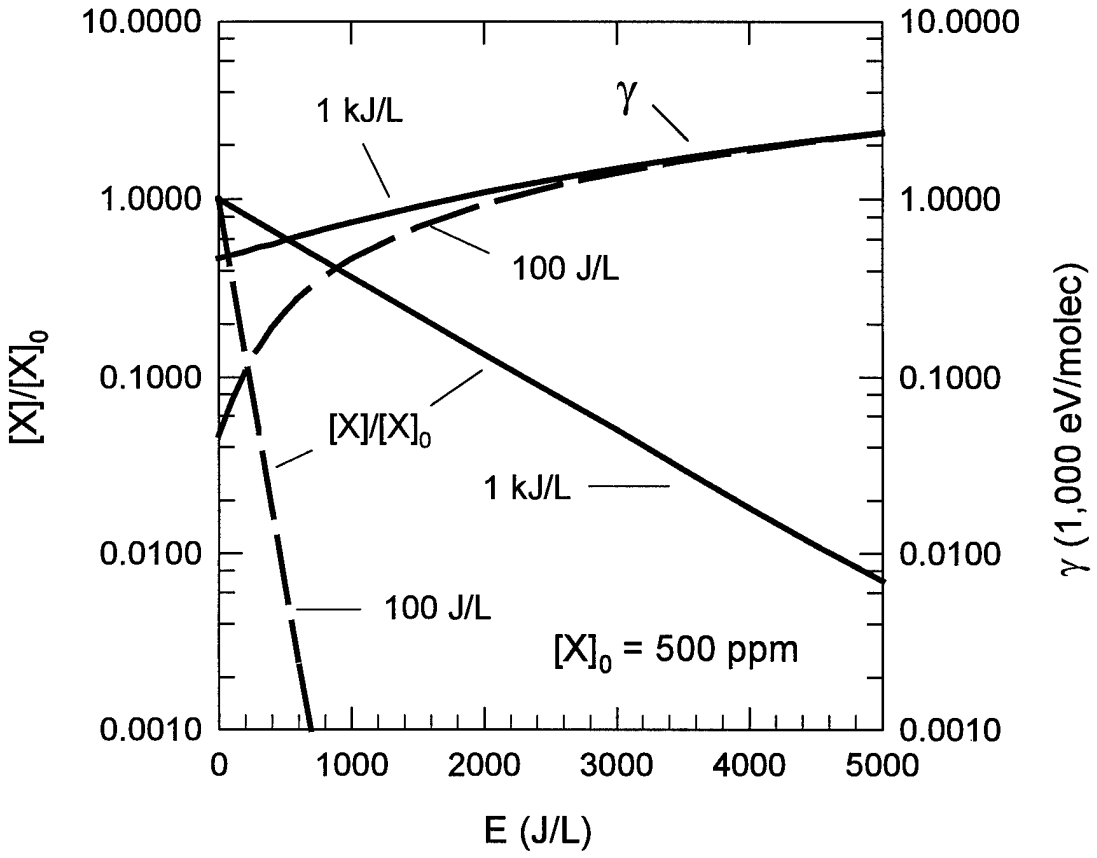
10.0000
1.0000
0.1000
0.0100
0.0010
[X]/[X]0
γ (1,000 eV/molec)
1 kJ/L
γ
100 J/L
[X]/[X]0
1 kJ/L
100 J/L
[X]0 = 500 ppm
0
1000
2000
3000
4000
5000
E (J/L)

Table 10.1: Example Radical Formation Mechanisms

Electron impact

$e + O_2 \rightarrow O + O^* + e$

$e + O_2 \rightarrow O + O + e$

$e + N_2 \rightarrow N + N + e$

$e + O_2 \rightarrow O_2^* + e$

$e + N_2 \rightarrow N_2^* + e$

$e + H_2O \rightarrow OH + H + e$

$e + NO \rightarrow N + O + e$

$e + NH_3 \rightarrow NH + H_2 + e$

Quenching

$O^* + H_2O \rightarrow 2OH$

$N_2^* + O_2 \rightarrow N_2 + O + O$

Ionization/Clusters

$e + O_2 \rightarrow O_2^+ + e$

$O_2^+ + H_2O \rightarrow O_2^+ (H_2O)$

$O_2^+ (H_2O) + H_2O \rightarrow HO_3^+ + O_2 + OH$

$O_2^+ (H_2O) + H_2O \rightarrow HO_3^+ (OH) + O_2$

$HO_3^+ (OH) + H_2O \rightarrow HO_3^+ + H_2O + OH$

Others

$H + O_3 \rightarrow OH + O_2$

$HO_2 + NO \rightarrow OH + NO_2$

$H + O_2 + M \rightarrow HO_2 + M$

$O + O_2 + M \rightarrow O_3 + M$